
THE LORENZ SYSTEM AND APPLICATIONS OF CHAOS

YEAR 3 PROJECT
SAMUEL HANCOCK

*Supervised by Waleed A Ali
Mathematical Sciences Department
University of Bath
2024*



ABSTRACT

The main objective of this project is to investigate the chaotic behaviour demonstrated by the Lorenz system. This project will look at the history and origins of our current understanding of chaos theory, building on thermodynamics and planetary motion and the development of the weather model suggested by Edward Lorenz. The Lorenz differential equations will be analysed from dynamical and numerical points of view to investigate the stability of their steady states and the behaviours they exhibit. Different parameter values will be studied that lead to stabilisation of chaotic behaviour and the production of bifurcation diagrams. Finally, some applications of chaotic systems will be explained.

Generative AI was used as an assistive tool for code alteration in Figure 27.

Contents

1	Introduction	3
1.1	A Brief History of Chaos	3
1.1.1	Maxwell and Sensitive Dependence On Initial Data	3
1.1.2	Poincaré and The Three-Body Problem	4
2	The Lorenz System	5
2.1	Origin of the Lorenz System	5
2.2	Steady States of the Lorenz System	5
2.2.1	Local Stability of the Origin	6
2.2.2	Global Stability of the Origin	7
2.2.3	Stability of the Non-Trivial Steady States	8
2.3	Studying the Lorenz Attractor	10
2.3.1	Attractors and Fractals	10
2.3.2	Numerical Experiments on the Lorenz Attractor	10
2.3.3	Lyapunov Exponents and Diverging Trajectories	13
2.3.4	Dynamics on the Lorenz Attractor	14
2.3.5	Homoclinic Bifurcation	16
2.3.6	Transient Chaos and Two Types of Attractor	19
2.3.7	Beyond the Hopf Bifurcation	22
3	Applications of Chaos	23
3.1	Chaotic Masking	23
3.2	Controlling Chaos	26
3.2.1	The OGY Method	26
3.2.2	OGY Method and Delay Coordinates	27
3.2.3	Estimation Techniques in the OGY Algorithm	28
3.3	Applications of Chaos Control	29
3.3.1	Cardiac Chaos Control and Targeting	29
3.3.2	Chaotic Control in Space Travel	31
4	Conclusion	31

1 Introduction

The Cambridge Dictionary defines *Chaos* as “A state of total confusion with no order” [1]. However, *Chaos Theory* is also a branch of mathematics describing the behaviour of dynamical systems that are highly sensitive to initial conditions. It explores the seemingly completely random patterns and phenomena that emerge from deterministic systems despite following precise rules. It has numerous applications in subjects such as physics, engineering, and biology which will be discussed in this project alongside the main focus, the Lorenz equations.

1.1 A Brief History of Chaos

Chaos theory is a relatively new field of study within mathematics, with the earliest mentions of chaos dating only to the 1860s and 1870s. This is largely because much of the mathematics involved in chaos theory involves the repeated iteration of simple mathematical formulae, which would be impractical to do by hand. Thus, the invention of electronic computers in the 1940s acted as a catalyst for chaos theory since it made these repeated calculations practical. Furthermore, coded figures and imaging made it possible to visualize chaotic systems.

1.1.1 Maxwell and Sensitive Dependence On Initial Data

James Clerk Maxwell (1831-1879) was a Scottish physicist who is mostly known for the formulation of the theory of electromagnetism and his distribution law for the velocities of gas molecules, leading to the Maxwell-Boltzmann distribution curve (Figure 1).

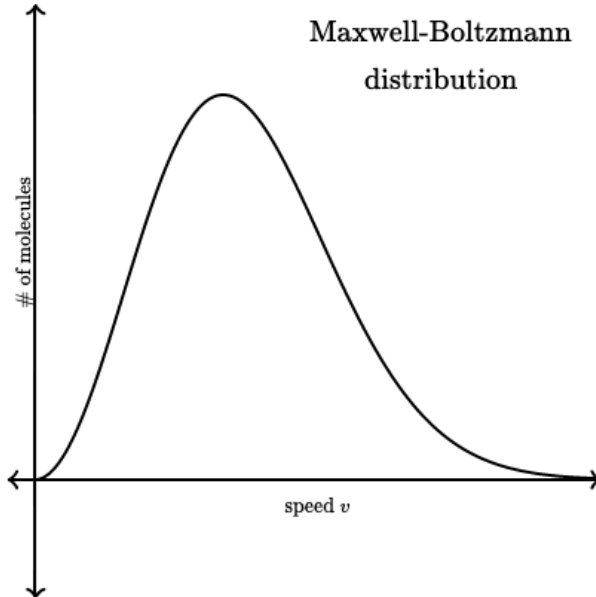


Figure 1: Maxwell-Boltzmann distribution curve.

It was in the latter of these that Maxwell discovered that sensitive dependence on initial data in the interactions between gas molecules was essential in producing statistical regularity [2]. This can be regarded as the first understanding of what chaos is, though there was no further detail than this until later that century.

1.1.2 Poincaré and The Three-Body Problem

The three-body problem is as follows: Consider the three bodies (planets) with vector positions $\mathbf{r}_i(t) = (x_i(t), y_i(t), z_i(t))$ and respective masses m_i for $i = 1, 2, 3$. By Newton's Law of Universal Gravitation, each planet is subjected to an attractive force by the other planets in the system. The forces are proportional to their masses and inversely proportional to the square of their distance (inverse-square law). Hence, using dot notation to represent derivatives with respect to time, by Newton's second law ($F = ma = m\ddot{\mathbf{r}}$), with G the gravitational constant, we have

$$\begin{aligned}\ddot{\mathbf{r}}_1 &= -Gm_2 \frac{\mathbf{r}_1 - \mathbf{r}_2}{|\mathbf{r}_1 - \mathbf{r}_2|^3} - Gm_3 \frac{\mathbf{r}_1 - \mathbf{r}_3}{|\mathbf{r}_1 - \mathbf{r}_3|^3} \\ \ddot{\mathbf{r}}_2 &= -Gm_3 \frac{\mathbf{r}_2 - \mathbf{r}_3}{|\mathbf{r}_2 - \mathbf{r}_3|^3} - Gm_1 \frac{\mathbf{r}_2 - \mathbf{r}_1}{|\mathbf{r}_2 - \mathbf{r}_1|^3} \\ \ddot{\mathbf{r}}_3 &= -Gm_1 \frac{\mathbf{r}_3 - \mathbf{r}_1}{|\mathbf{r}_3 - \mathbf{r}_1|^3} - Gm_2 \frac{\mathbf{r}_3 - \mathbf{r}_2}{|\mathbf{r}_3 - \mathbf{r}_2|^3}\end{aligned}$$

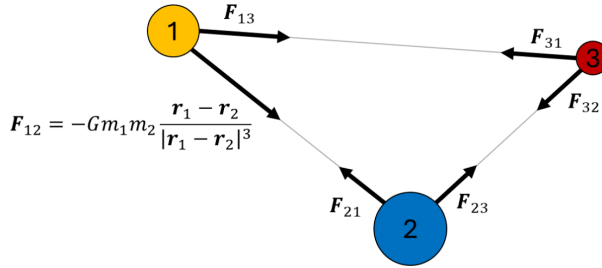


Figure 2: Forces in the three-body problem.

The three-body problem can be visualised as in Figure 2 with two example larger bodies (labelled 1 and 2) and a relatively smaller body (labelled 3). The force that body i exerts on body j is represented by

$$\mathbf{F}_{ij} = -Gm_i m_j \frac{\mathbf{r}_i - \mathbf{r}_j}{|\mathbf{r}_i - \mathbf{r}_j|^3}$$

Since each of the three planets has three degrees of freedom in three-dimensional space, we have nine differential equations to solve. Since acceleration is the second derivative of the position vector, the equations are second order. Due to the complexity of the problem, solutions can generally only be found via numerical methods.

The restricted three-body problem is a simplification of the general version where one of the bodies is assumed to have negligible mass. Thus, the force that this smaller “planetoid” exerts on the two massive bodies may be neglected and the system can be analysed in terms of two-body motion [3] - hence the name restricted.

Henri Poincaré (1854-1912) was a French mathematician and theoretical physicist whose work on the three-body problem in the 1890s established the existence of an infinite number of periodic solutions to the restricted three-body problem [4]. By utilising *Poincaré sections*, he was able to study the qualitative behaviour of the system and investigate the stability of the chaotic dynamics of this problem.

2 The Lorenz System

2.1 Origin of the Lorenz System

Edward Lorenz (1917-2009) was an American mathematician and meteorologist who was responsible for the true birth of chaos theory. Whilst working on numerical weather prediction, Lorenz started simulating weather patterns based on twelve variables, representing factors such as temperature and wind speed. While attempting to replicate one particular simulation, Lorenz took a shortcut and entered rounded-off data from halfway through a previous run (three decimal places) into the computer, which worked with higher precision (six decimal places) [5]. The output was entirely different, leading Lorenz to believe that this system of equations had sensitive dependence on initial conditions. Lorenz furthered his research on this topic, leading him to publish a paper in 1963 titled “Deterministic Nonperiodic Flow” [6]. In this, there was a very simplified model of convection, known as the “Lorenz system”. The system is as follows:

$$\begin{aligned}\frac{dx}{dt} &= \sigma(y - x) \\ \frac{dy}{dt} &= x(\rho - z) - y \\ \frac{dz}{dt} &= xy - \beta z\end{aligned}$$

In the original meteorological context, the equations relate to a two-dimensional fluid layer uniformly warmed from below and cooled from above. Here x represents the rate of convection, y the horizontal temperature variation, and z the vertical temperature variation. The constants σ , ρ , and β are all assumed to be positive and are respectively the Prandtl number (ratio of fluid viscosity to thermal conductivity), Rayleigh number (associated with buoyancy-driven motion when subjected to a temperature gradient), and a number characterising the physical dimensions of the layer.

For parameter values $\sigma = 10$, $\rho = 28$ and $\beta = \frac{8}{3}$, the long-term behaviour of the system is an aperiodic attractor (to be defined later).

2.2 Steady States of the Lorenz System

To analyse the behaviour of the Lorenz system we must first look at the fixed points of the system. These occur when

$$\frac{dx}{dt} = \frac{dy}{dt} = \frac{dz}{dt} = 0$$

First notice that $(0, 0, 0)$ is a fixed point of the system. Then, calculating non-trivial fixed points yields:

$$\frac{dx}{dt} = 0 \Rightarrow x = y$$

Substituting this into the equation for $\frac{dy}{dt}$:

$$\Rightarrow x(\rho - z - 1) = 0$$

$$\Rightarrow z = \rho - 1$$

Substituting this into the equation for $\frac{dz}{dt}$:

$$\Rightarrow x^2 - \beta(\rho - 1) = 0$$

$$\Rightarrow x = \pm\sqrt{\beta(\rho - 1)}$$

Hence the trivial steady state $(0, 0, 0)$ and two non-trivial steady states are given by:

$$C^+ = (\sqrt{\beta(\rho - 1)}, \sqrt{\beta(\rho - 1)}, \rho - 1)$$

$$C^- = (-\sqrt{\beta(\rho - 1)}, -\sqrt{\beta(\rho - 1)}, \rho - 1)$$

The non-trivial steady states exist for $\rho > 1$ since all the steady states must be real-valued in this physical application.

2.2.1 Local Stability of the Origin

By linearisation about the trivial fixed point, we can further analyse the Lorenz system. We do this by looking at the eigenvalues of the Jacobian matrix evaluated at the point $(0, 0, 0)$. The Jacobian matrix for the Lorenz system is given by

$$J(x, y, z) = \frac{\partial(\dot{x}, \dot{y}, \dot{z})}{\partial(x, y, z)} = \begin{pmatrix} \frac{\partial \dot{x}}{\partial x} & \frac{\partial \dot{x}}{\partial y} & \frac{\partial \dot{x}}{\partial z} \\ \frac{\partial \dot{y}}{\partial x} & \frac{\partial \dot{y}}{\partial y} & \frac{\partial \dot{y}}{\partial z} \\ \frac{\partial \dot{z}}{\partial x} & \frac{\partial \dot{z}}{\partial y} & \frac{\partial \dot{z}}{\partial z} \end{pmatrix} = \begin{pmatrix} -\sigma & \sigma & 0 \\ \rho - z & -1 & -x \\ y & x & -\beta \end{pmatrix}$$

Hence, when evaluated at the origin, the Jacobian becomes

$$J(0, 0, 0) = \left. \begin{pmatrix} -\sigma & \sigma & 0 \\ \rho - z & -1 & -x \\ y & x & -\beta \end{pmatrix} \right|_{(0,0,0)} = \begin{pmatrix} -\sigma & \sigma & 0 \\ \rho & -1 & 0 \\ 0 & 0 & -\beta \end{pmatrix}$$

We can now find the eigenvalues of this matrix by calculating the characteristic polynomial $P(\lambda)$ using the formula $P(\lambda) = -\det(J - \lambda I)$, where I is the identity matrix. Hence, we obtain

$$P(\lambda) = \begin{vmatrix} -\sigma - \lambda & \sigma & 0 \\ \rho & -1 - \lambda & 0 \\ 0 & 0 & -\beta - \lambda \end{vmatrix} = -(\beta + \lambda)(\lambda^2 + (\sigma + 1)\lambda + \sigma(1 - \rho))$$

$$\Rightarrow \lambda_1 = -\beta, \lambda_{\pm} = \frac{-(\sigma + 1) \pm \sqrt{(\sigma + 1)^2 - 4\sigma(1 - \rho)}}{2}$$

where λ_{\pm} are real since $D = (\sigma + 1)^2 - 4\sigma(1 - \rho) = (\sigma - 1)^2 + 4\sigma\rho > 0$, for all $\sigma, \rho > 0$.

Now we must consider separate cases for D to classify the trivial steady state ¹

- For $0 < \rho < 1$, $\sqrt{D} < \sigma + 1$ which implies $\lambda_{\pm} < 0$. Thus, all three eigenvalues are negative and the origin is a sink, or stable node. (See Figure 3(left)).

¹Recall that the signs of the eigenvalues of the Jacobian determine the stability as follows:

- If all the eigenvalues are positive, then the steady state is an unstable node;
- If all the eigenvalues are negative, then the steady state is a stable node;
- If the eigenvalues are of different signs, then the steady state is a saddle;
- If at least one of the eigenvalues is 0, then further investigation needs to be conducted linear stability analysis or visual investigation.

2. For $\rho > 1$, $\sqrt{D} > \sigma + 1$ which implies there are two negative eigenvalues and one positive eigenvalue, conveying that the origin is a saddle point. This means that solution trajectories in some directions converge towards the origin and in other directions move away from the origin. (See Figure 3(right)).
3. At $\rho = 1$, the eigenvalues are $0, -(\sigma + 1), -\beta$. As 0 is an eigenvalue, more work needs to be done to determine local stability. The qualitative change in stability as ρ passes through 1 along with the birth of two new fixed points at $\rho = 1$ (C^+ and C^-) indicates that $\rho = 1$ is a supercritical pitchfork bifurcation point.

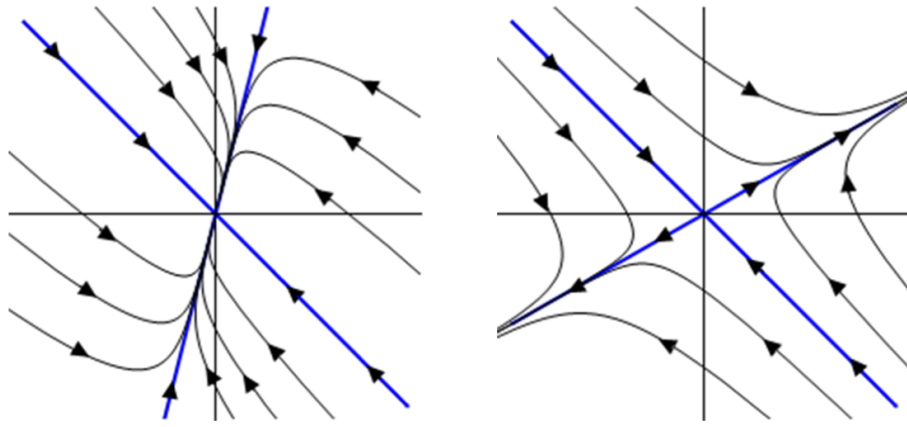


Figure 3: Generic 2D representation of the origin as a sink (left) and a saddle (right). ‘Inward-pointing’ arrows are associated with negative eigenvalues. ‘Outward-pointing’ arrows are associated with positive eigenvalues.

2.2.2 Global Stability of the Origin

Firstly, we analyse the global stability of the origin for $0 < \rho < 1$. We do this by considering a Lyapunov (continuously differentiable and positive definite) function of the form

$$V(x(t), y(t), z(t)) = V(\mathbf{x}) = \frac{1}{\sigma}x^2 + y^2 + z^2$$

The level sets of $V(\mathbf{x})$ are ellipsoids centred at the origin. Figure 4 shows an example of what the function would look like for $V = 1$.

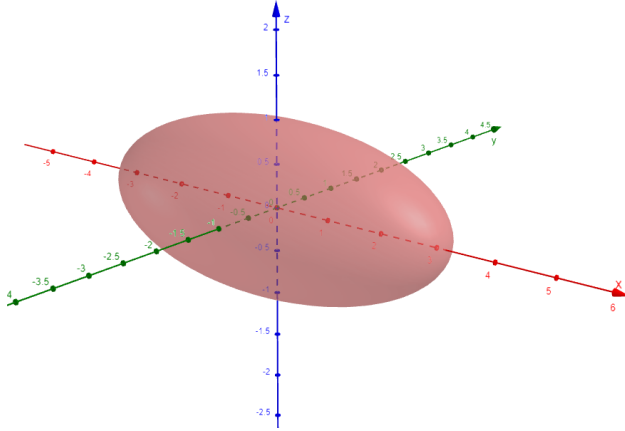


Figure 4: Example level set of $V(\mathbf{x}) = 1$ for $\sigma = 10$.

The stability of the origin can then be shown by using the *Lyapunov Stability Theorem* [7]. This states that if there exists $V(\mathbf{x})$ with the following properties:

- $V(\mathbf{x}) > 0$, for all \mathbf{x} except at the fixed point where $V(\mathbf{x}) = 0$,
- $\dot{V}(\mathbf{x}) \leq 0, \forall \mathbf{x}$,

then the fixed point of the system is stable. Hence, for our chosen $V(\mathbf{x})$ we have

$$\begin{aligned}\dot{V}(\mathbf{x}) &= \frac{2}{\sigma}x\dot{x} + 2y\dot{y} + 2z\dot{z} \\ &= 2\left((\rho+1)xy - x^2 - y^2 - \beta z^2\right) \\ &= -2\left(x - \left(\frac{\rho+1}{2}\right)y\right)^2 - 2\left(1 - \left(\frac{\rho+1}{2}\right)^2\right)y^2 - 2\beta z^2 < 0\end{aligned}$$

Since for $0 < \rho < 1$, $1 - \left(\frac{\rho+1}{2}\right)^2 > 0$. Therefore $V(\mathbf{x})$ is a strictly decreasing Lyapunov function for all values $(x(t), y(t), z(t))$. Thus, solutions tend to the origin as $t \rightarrow \infty$. This means that for $0 < \rho < 1$, the origin is globally stable and we do not get “interesting” behaviour with regards to the Lorenz attractor.

As previously shown, the origin is unstable for $\rho > 1$, and now C^+ and C^- exist. It can be shown that these fixed points are stable for values $1 < \rho < \rho_H$ where ρ_H is a stability threshold value of ρ (which will be discussed later).

2.2.3 Stability of the Non-Trivial Steady States

We begin the stability analysis of C^+ and C^- by first recognising that the Lorenz system is symmetric under an inversion in the z -axis i.e. if $(x(t), y(t), z(t))$ is a solution, then so is $(-x(t), -y(t), z(t))$. Thus, when considering the two remaining equilibrium points, we need only analyse one of them as the same properties will be true of the other. Therefore, without loss of generality, consider the steady state, C^+ , which only exists for $\rho > 1$:

$$J(C^+) = \left. \begin{pmatrix} -\sigma & \sigma & 0 \\ \rho - z & -1 & -x \\ y & x & -\beta \end{pmatrix} \right|_{C^+} = \begin{pmatrix} -\sigma & \sigma & 0 \\ 1 & -1 & -\sqrt{\beta(\rho-1)} \\ \sqrt{\beta(\rho-1)} & \sqrt{\beta(\rho-1)} & -\beta \end{pmatrix}$$

The eigenvalues of $J(C^+)$ are the roots of the characteristic polynomial

$$P(\lambda) = \lambda^3 + (\beta + \sigma + 1)\lambda^2 + \beta(\sigma + \rho)\lambda + 2\beta\sigma(\rho - 1) = 0$$

By the Fundamental Theorem of Algebra [8], we know that at least one root of the cubic equation, λ_1 , must be real. Now, differentiating the polynomial yields:

$$P'(\lambda) = 3\lambda^2 + 2(\beta + \sigma + 1)\lambda + \beta(\sigma + \rho) > 0, \quad \forall \lambda \geq 0$$

This implies that $P(\lambda)$ is an increasing function for $\lambda \geq 0$ and since $P(0) > 0$, we can conclude that any real root of the cubic equation is necessarily negative (as the cubic coefficient is positive).

It is easier to check numerically whether the remaining roots, $\lambda_{2,3}$, are real or complex since analytical methods would likely require the cubic formula. When typical parameter values of the Lorenz system are used, $(\sigma, \beta, \rho) = (10, \frac{8}{3}, 28)$, $\lambda_{2,3}$ are real for $\rho < 1.3456$ and complex otherwise [9].

Now suppose that λ_2 and λ_3 are in fact complex. That is they are of the form $a \pm \omega i$, $\omega \neq 0$. Note that the roots must be a complex conjugate pair (again by the Fundamental Theorem of Algebra). To find the stability of C^+ , we must consider $\text{Re}(\lambda_{2,3})$:

- If $a < 0$, all the eigenvalues of $J(C^+)$ have a negative real part, hence the non-trivial steady states are stable focus-nodes. This is the term used when the equilibrium point has one real eigenvalue and a pair of complex-conjugate eigenvalues, and all eigenvalues have real parts of the same sign [10].
- If $a > 0$, J has one negative real eigenvalue and two complex eigenvalues with a positive real part. This implies that C^+ and C^- are unstable saddle-foci.
- At $a = 0$, there is a stability boundary; so we will investigate for which values of ρ this occurs.

$$\begin{aligned}
P(\omega i) &= (\omega i)^3 + (\beta + \sigma + 1)(\omega i)^2 + \beta(\sigma + \rho)(\omega i) + 2\beta\sigma(\rho - 1) = 0 \\
&\Rightarrow \left(-\omega^2(\beta + \sigma + 1) + 2\beta\sigma(\rho - 1) \right) + \left(-\omega(\omega^2 - \beta(\sigma + \rho)) \right)i = 0 \\
&\Rightarrow \begin{cases} \omega^2 - \beta(\sigma + \rho) = 0 \\ -\omega^2(\beta + \sigma + 1) + 2\beta\sigma(\rho - 1) = 0 \end{cases} \tag{1}
\end{aligned}$$

Solving the equations by eliminating ω yields:

$$\rho = \rho_H = \frac{\sigma(\sigma + \beta + 3)}{\sigma - \beta - 1}, \quad \sigma > \beta + 1$$

Experimentally, we observe that for $\rho < \rho_H$, all three eigenvalues of $J(C^+)$ will have a negative real part so C^+ and C^- will be stable, whereas for $\rho > \rho_H$, $J(C^+)$ has one negative real eigenvalue and a pair of complex conjugate eigenvalues with positive real parts, indicating instability (a saddle point is considered unstable).

The eigenvalues crossing the imaginary axis indicates the existence of a *Hopf bifurcation* for $\rho = \rho_H$; a phenomenon which occurs when a periodic solution or limit cycle surrounding an equilibrium point arises or diminishes as a parameter (in this case ρ) varies. This particular Hopf bifurcation is subcritical, meaning that as $\rho \rightarrow \rho_H$ from below, the limit cycle shrinks around the fixed point. At the Hopf bifurcation, the fixed point absorbs the cycle, becoming a saddle point. Then, as ρ continues to increase beyond ρ_H , trajectories must fly off to a distant attractor.

Based on the analysis so far, we have the partial bifurcation diagram as shown in Figure 5:

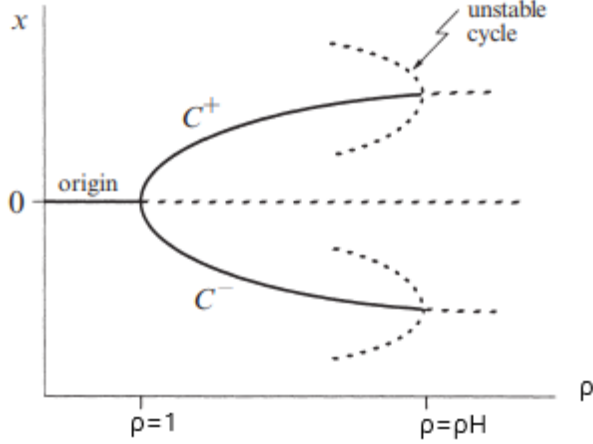


Figure 5: Partial bifurcation diagram of Lorenz system showing supercritical pitchfork and subcritical Hopf bifurcations at $\rho = 1$ and $\rho = \rho_H$, respectively. [11]

2.3 Studying the Lorenz Attractor

2.3.1 Attractors and Fractals

To understand the behaviours of solutions of the Lorenz system, first, it is important to understand the concept of attractors. In simple terms, an *attractor* can be described as a set to which solution trajectories of a dynamical system eventually converge. More formally, an attractor is defined to be a closed set A with the following properties:

- *A is an invariant set*: any trajectory $\mathbf{x}(t)$ that starts in A stays in A for all time
- *A attracts an open set of initial conditions*: there is an open set U containing A such that if $\mathbf{x}(0) \in U$, then $|\mathbf{x}(t) - A| \rightarrow 0$ as $t \rightarrow \infty$. This means that A attracts all trajectories that start sufficiently close to it. The largest such U is called the *basin of attraction* of A .
- *A is minimal*: there is no proper subset of A that satisfies the first two properties [12].

Attractors can be simple, for example, fixed points and limit cycles, or more complicated geometric structures. If an attractor has a fractional dimension, the shape is called a *fractal* and the attractor is labelled *strange*. The table below summarises different types of attractors:

Type of Attractor	State	Examples
Point Attractor	Stable	Equilibrium position of a pendulum at rest
Limit Cycles	Oscillatory	Rhythm of a beating heart
Torus Attractor	Quasi-periodic	Motion of a planet
Strange Attractor	Complex chaotic motion	Lorenz Attractor, explaining convection roll phenomena

Quasiperiodicity is the property of a system that displays irregular periodicity.

2.3.2 Numerical Experiments on the Lorenz Attractor

To see the long-term behaviour of trajectories, Lorenz used numerical integration and for the case of $\sigma = 10, \beta = \frac{8}{3}, \rho = 28$, he noticed some strange properties. The choices of σ and β here are thought to roughly represent atmospheric conditions, so these often remain fixed when studying the Lorenz system. In this particular case, $\rho_H \approx 24.74$ so notice that this value of ρ is beyond the Hopf bifurcation point. Hence,

due to our previous analysis, we expect strange behaviour to occur. Using the initial conditions $(0, 1, 0)$, starting near the saddle point at the origin, we obtain the following time series graph for y against t using MATLAB:

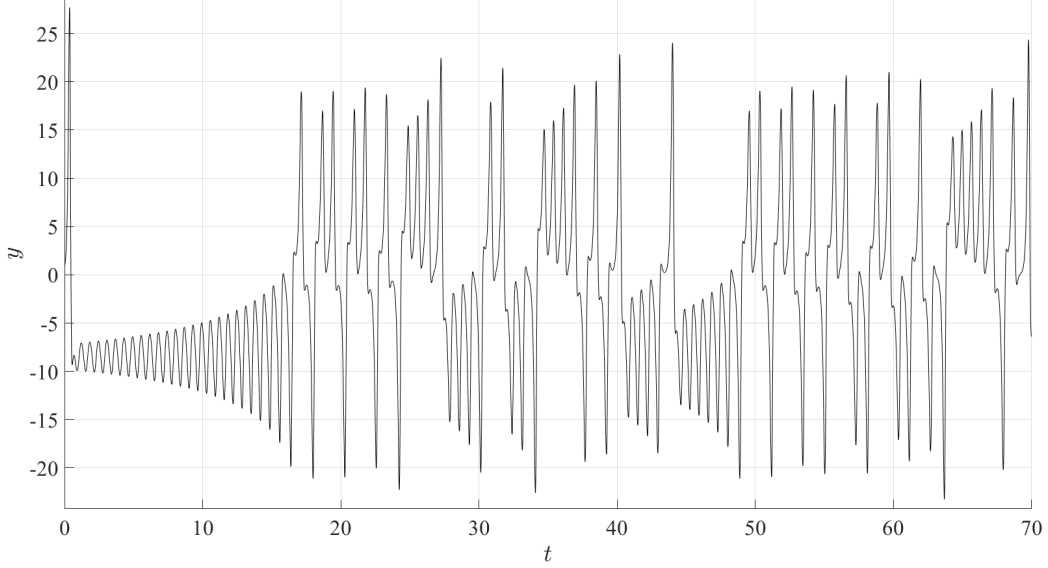


Figure 6: Time series graph of y against t for the Lorenz system with parameter values $\sigma = 10$, $\beta = \frac{8}{3}$, $\rho = 28$ and initial conditions $(0, 1, 0)$.

Figure 6 shows that after brief ‘normal-looking’ behaviour, the solution starts to oscillate erratically and aperiodically. Though sections of the graph may appear similar, the oscillatory patterns are all unique and this behaviour continues without repetition as $t \rightarrow \infty$. Graphs for x against t and z against t display similar, irregular behaviour.

Furthermore, we can show that the Lorenz attractor is chaotic by showing that the system displays sensitive dependence on initial conditions. By plotting the time series graph of y against t again in Figure 7, but this time with the initial conditions $(0, 1.00001, 0)$; and comparing it to the previous initial conditions of $(0, 1, 0)$ we can see the significant differences between the two trajectories despite only a minor difference of 10^{-5} in the y -coordinate.

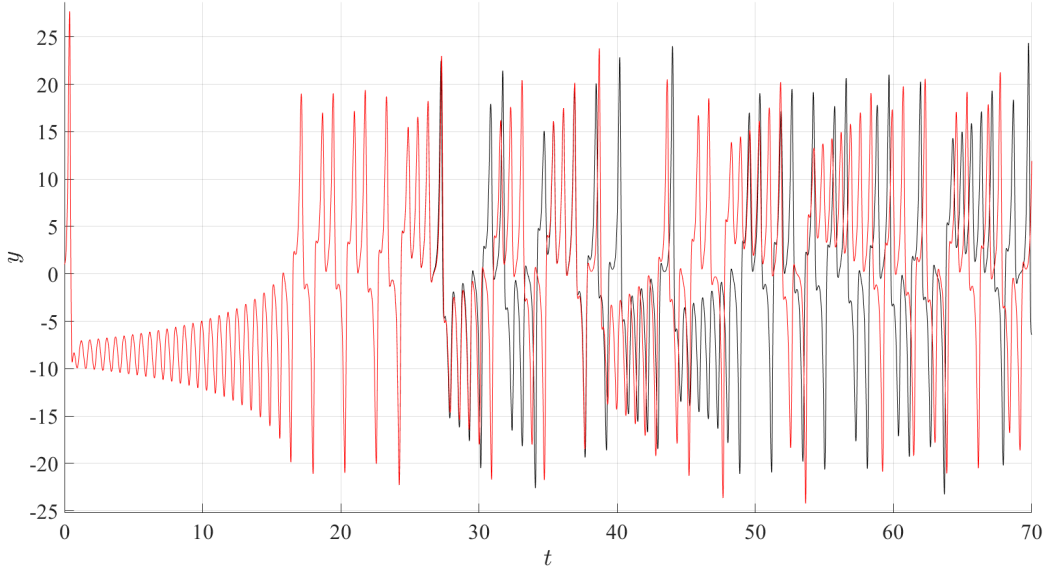


Figure 7: Time series graph of y against t for the Lorenz system with parameter values $\sigma = 10, \beta = \frac{8}{3}, \rho = 28$ and initial conditions $(0, 1, 0)$ (black) and $(0, 1.00001, 0)$ (red).

We can now visualise the attractor in three dimensions, as shown in Figure 8, to gain a better understanding of the solution to the system.

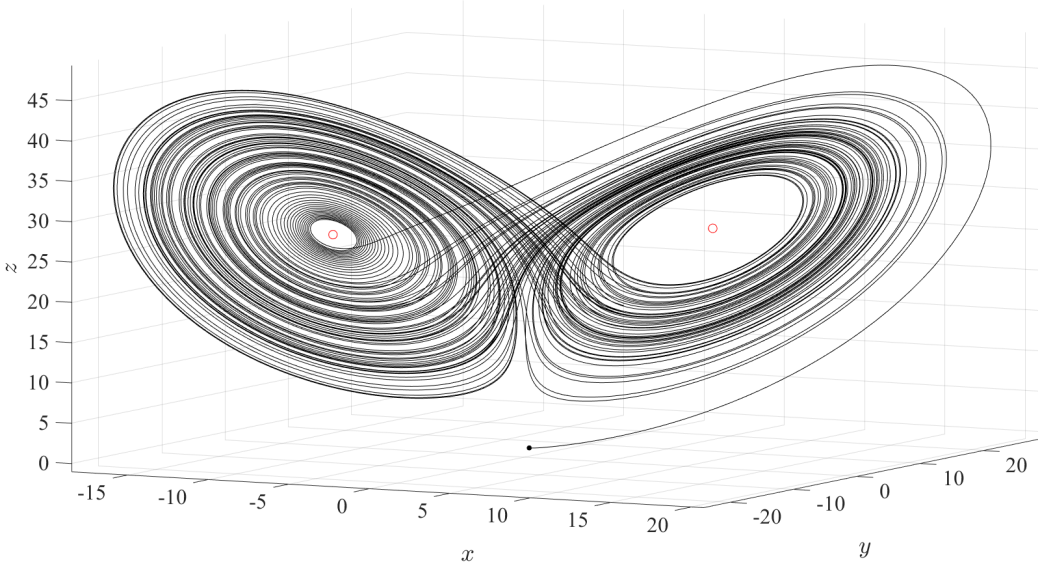


Figure 8: 3D plot of the Lorenz system with parameter values $\sigma = 10, \beta = \frac{8}{3}, \rho = 28$, initial conditions $(0, 1, 0)$ (shown as a solid dot) and $t \in [0, 100]$. Non-trivial equilibria are displayed in red.

The trajectory shown in Figure 8 initially sweeps to the right, then left; spirals around one equilibrium point, before flying off to the other non-trivial equilibrium point; spiralling there, before flying off to the left again. This behaviour repeats itself for an infinite time with the number of spirals made around each fixed point being unpredictable for each cycle. The attractor looks like a pair of butterfly wings. This, coupled

with the sensitive dependence on initial conditions, led Lorenz to coin the term “butterfly effect”; a concept derived from the metaphorical example in which details of a tornado were influenced by small perturbations such as the flapping of the wings of a distant butterfly.

The Lorenz attractor is also strange since it has a Hausdorff dimension of approximately 2.06 [13]. This value can be obtained using converging box counting algorithms, among other methods. Thus, the Lorenz attractor is considered to be both strange and chaotic.

2.3.3 Lyapunov Exponents and Diverging Trajectories

Lyapunov exponents can be used to further illustrate the chaotic behaviours of the Lorenz system. The Lyapunov exponent of a dynamical system is a measure of the rate of divergence of infinitesimally close trajectories.

Formally, for an n -dimensional dynamical system, the Lyapunov exponents λ_i are defined as the average rates of exponential growth or decay of infinitesimal perturbations along each direction in phase space.

Mathematically, if $\delta(t)$ represents the deviation vector between two nearby trajectories at time t , then the growth of $\delta(t)$ in each direction can be approximated by $|\delta(t)| \approx |\delta_0|e^{\lambda_i t}$ for each i , where δ_0 is the initial separation of trajectories. The Lyapunov exponents are the λ_i terms.

In the context of chaotic systems like the Lorenz system, positive Lyapunov exponents indicate exponential divergence of nearby trajectories, implying sensitive dependence on initial conditions and the presence of chaotic behaviour. Conversely, negative Lyapunov exponents indicate convergence, suggesting stability or regular behaviour. The largest (maximal) Lyapunov exponent (MLE) often characterises the system’s level of chaos: a positive MLE typically signifies chaotic dynamics.

To estimate the MLE of the Lorenz system, we can plot $\ln |\delta(t)|$ against t to obtain roughly a straight line with a positive slope λ_{MLE} . Using MATLAB, the following graph was created to estimate the MLE with an initial perturbation of 10^{-9} in z .

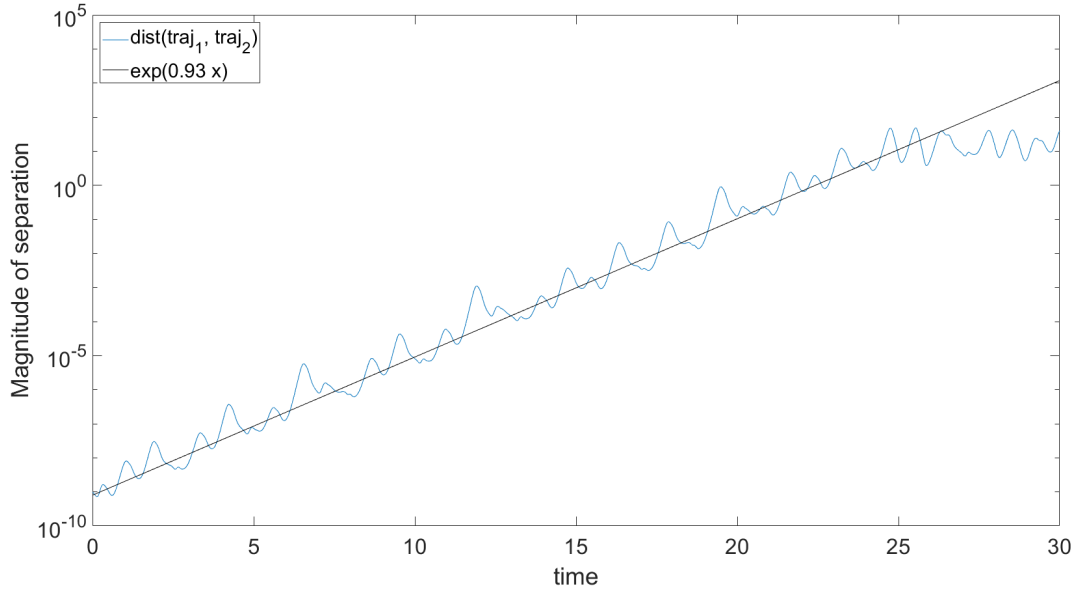


Figure 9: Graph showing the magnitude of separation of nearby Lorenz trajectories using initial conditions $(2, 3, 14)$ and an initial separation of $(0, 0, 10^{-9})$.

From the graph, the estimated value of the slope is 0.9341. The actual value of the MLE for the Lorenz system has been computed to be around 0.9056, making this estimate quite accurate. As this number is positive, we have verified that the Lorenz system exhibits sensitive dependence on initial conditions and therefore is chaotic.

You may notice that after $t \approx 25$, the curve starts to level off. This can be explained by the bounded nature of trajectories on the Lorenz attractor. It is only possible for solutions to diverge as far as the dimensions of the attractor itself.

2.3.4 Dynamics on the Lorenz Attractor

By reducing his system to a 1D map, Lorenz further analysed the dynamics of his strange attractor. He showed that periodic orbits and limit cycles on his attractor were unstable, implying true chaotic behaviour, as some had suggested the possibility that what Lorenz was observing was just extremely long periodic orbits.

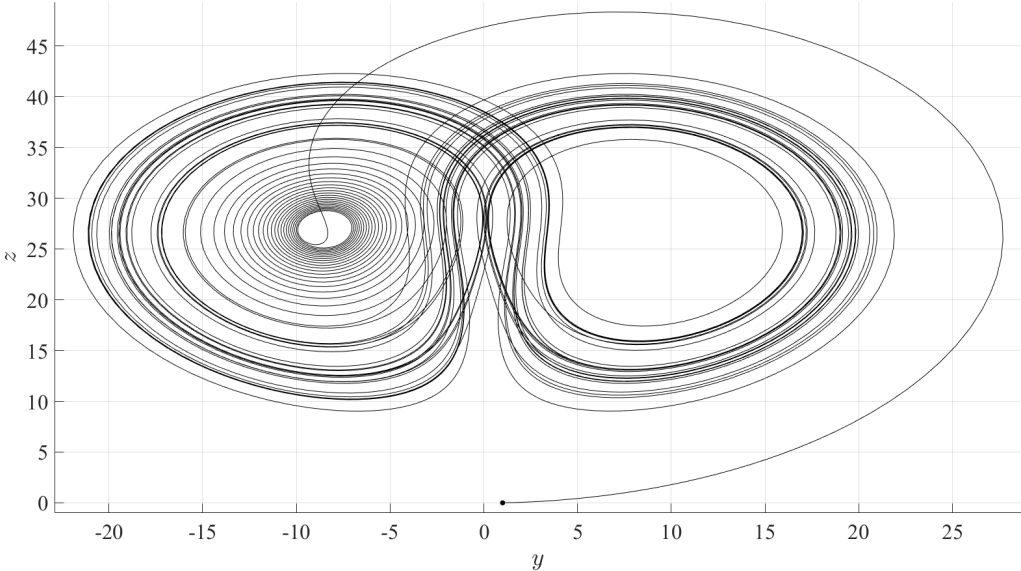


Figure 10: yz -plane for Lorenz system with initial conditions $(0, 1, 0)$ and parameter values $\sigma = 10, \beta = \frac{8}{3}, \rho = 28$.

Figure 10 shows the yz -plane for a particular case of the Lorenz system. From this plot, Lorenz stated in his paper:

“The trajectory apparently leaves one spiral only after exceeding some critical distance from the center. Moreover, the extent to which this distance is exceeded appears to determine the point at which the next spiral is entered; this in turn seems to determine the number of circuits to be executed before changing spirals again. It therefore seems that some single feature of a given circuit should predict the same feature of the following circuit.” [6]

The feature that Lorenz speaks of is the n^{th} local maximum of $z(t)$, denoted by z_n .

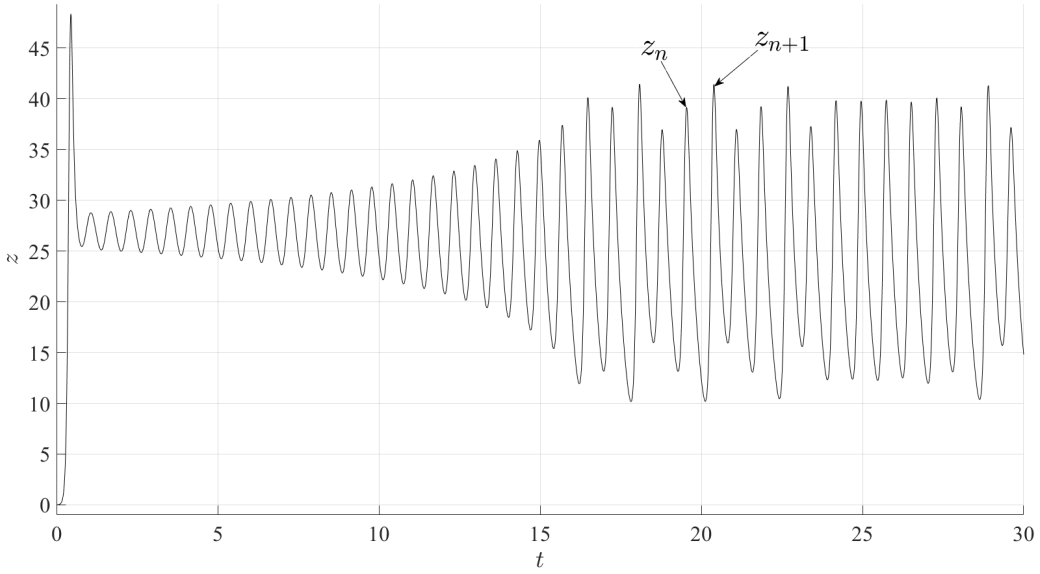


Figure 11: Time series graph of z against t , showing the maximum value of z at the n^{th} and $(n+1)^{\text{th}}$ cycles.

Lorenz postulated that z_n could be used to predict z_{n+1} . After numerical integration and measuring the local maxima of $z(t)$, Lorenz was able to come up with the plot shown in Figure 12:

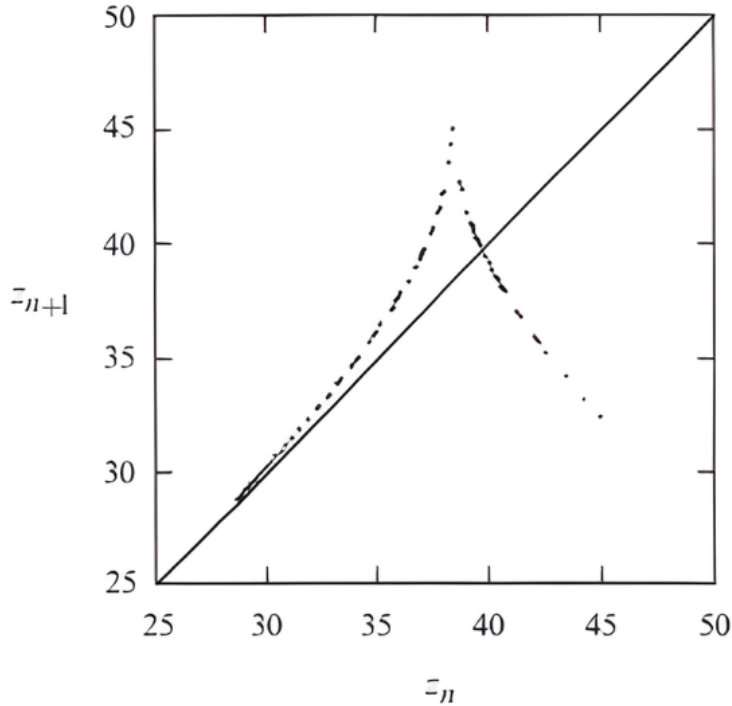


Figure 12: Plot of z_{n+1} vs z_n . [11]

Amazingly, the points seem to fall on a curve with almost no thickness. This means that the points plotted on the graph appear to form a continuous and smooth curve, allowing us to perform some analysis of the results. Hence, one could write $z_{n+1} = f(z_n)$ for some function f . We call this 1D map the *Lorenz*

map, with the shape of the curve resembling the *tent map* - another chaotic map.

From Figure 12, we can see that the straight line $z_{n+1} = z_n$ has been included. This line has a gradient of 1 and from the graph, we can see that $|f'(z)| > 1$, for all z . This is important as it means that limit cycles (providing they exist) are unstable. Further, one observes that there is an intersection between f and the line $z_{n+1} = z_n$, implying the existence of a fixed point $z^* = f(z^*)$. Geometrically, this can be represented by a closed periodic orbit of a similar shape to the orbits shown in Figure 10.

To prove that this periodic orbit is unstable, we let $z_n = z^* + \eta_n$, where $|\eta_n| \ll 1$ is a small trajectory perturbation. Hence, $z_{n+1} = f(z_n) = f(z^* + \eta_n)$. Performing a Taylor series expansion yields $f(z^*) + \eta_n f'(z^*) + \mathcal{O}(\eta_n^2)$ where we can ignore the last term since η_n is assumed to be very small.

Additionally, $z_{n+1} = z^* + \eta_{n+1}$. Equating the expressions implies $z^* + \eta_{n+1} \approx f(z^*) + \eta_n f'(z^*)$. But $z^* = f(z^*)$, hence $\eta_{n+1} \approx \eta_n f'(z^*)$. Recall that $|f'(z^*)| > 1$ which implies $|\eta_{n+1}| > |\eta_n|$. This means that the closed orbit z^* is unstable as the perturbation η_n grows with each iteration. This idea can be extended to show that any periodic orbit is unstable on the Lorenz attractor.

Suppose that a periodic sequence of the Lorenz map exists; z_0, z_1, z_2, \dots with $z_{n+p} = z_n$, for some integer $p \geq 1$. Consider a period-2 orbit of this form ($p = 2$). A point z on this orbit is a fixed point of $F := f^2$. Hence $z = f^2(z)$, and

$$\left| (F(z))' \right| = \left| (f^2(z))' \right| = \left| \frac{d}{dz}(f(f(z))) \right|$$

Using the chain rule;

$$= \left| f'(f(z)) f'(z) \right| = \underbrace{\left| f'(f(z)) \right|}_{>1} \underbrace{\left| f'(z) \right|}_{>1} > 1$$

Using the previous result that $f'(z) > 1$, for all z . We have now shown that this period-2 orbit is unstable from the properties of discrete maps. This process works similarly in cases of higher values of p and we conclude that for any p , period- p points of the Lorenz map are unstable. Thus, there are no stable periodic orbits for this case; verifying the chaotic and strange nature of the Lorenz attractor.

2.3.5 Homoclinic Bifurcation

A *manifold* can be described as a generalisation and abstraction of the notion of a curved surface. This means that any object that is nearly ‘flat’ on a small scale can be labelled a manifold even if after global modelling, the object clearly is not flat. A 2D sphere would be an example of a manifold - the boundary of a sphere.

Consider the Lorenz system with $\sigma = 10$, $\beta = \frac{8}{3}$. When $\rho > 1$, there is a two-dimensional sheet of initial values in \mathbb{R}^3 from which trajectories tend towards the origin. This is known as the stable manifold of the origin and near the origin it looks like a plane which is associated with the two negative eigenvalues of the system. There is also an unstable one-dimensional manifold related to the positive eigenvalue of the system at the origin. When ρ is only moderately larger than one, the stable manifold of the origin appears to divide \mathbb{R}^3 in a simple way; trajectories starting in one half-space tend towards C^+ and trajectories starting in the other half-space tend towards C^- . Trajectories on the stable manifold of the origin tend, unsurprisingly, to the origin.

As ρ increases towards a critical value, say ρ_b , the behaviour of trajectories fundamentally changes. The spirals formed by the trajectories starting on the unstable manifold of the origin grow larger with increasing ρ . For $\rho > \rho_b$ the trajectories “cross over” and are attracted to the “other” equilibrium point.

Talk of these manifolds is very abstract as their influence on trajectory behaviours is still not fully understood. What we do know is that the stable manifold is probably twisted strangely, looks flat near the origin, and includes the whole z -axis. Figure 13 and Figure 14 show trajectories along the unstable manifold in the cases $1 < \rho < \rho_b$ and $\rho > \rho_b$. Note that here C_1 and C_2 represent C^- and C^+ .

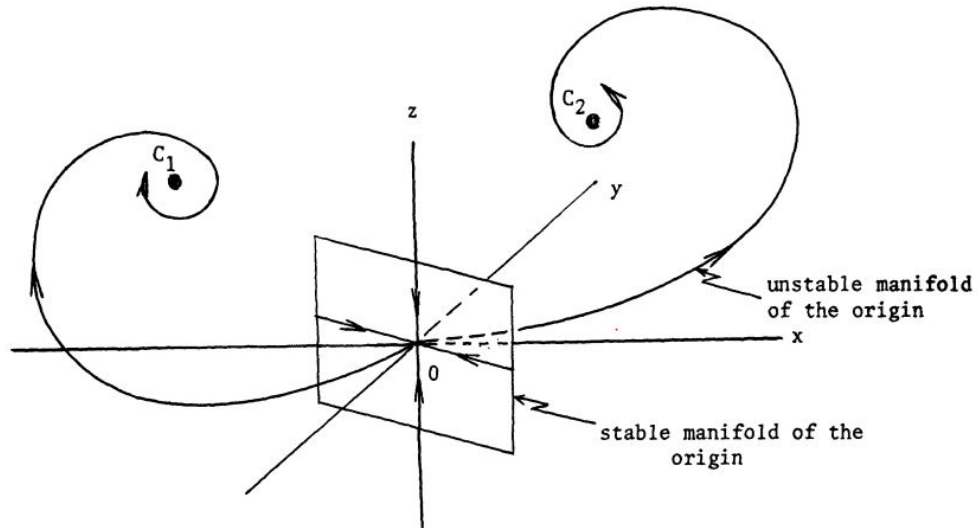


Figure 13: Behaviour of trajectories for $1 < \rho < \rho_b$. [14]

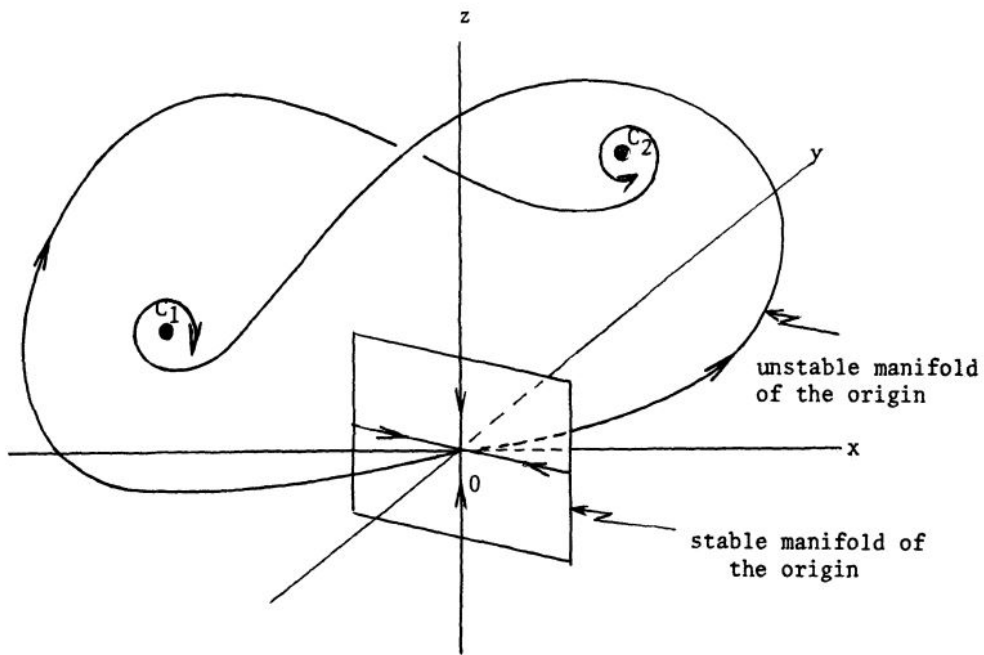


Figure 14: Behaviour of the unstable manifold for $\rho > \rho_b$. [14]

We can also use MATLAB to show this strange behaviour and locate ρ_b . Using the same initial conditions on both graphs for the black and red curves, respectively, while only changing ρ from 13.926 to 13.927 we

can illustrate the location of ρ_b and the critical role that it plays in altering the paths of trajectories.

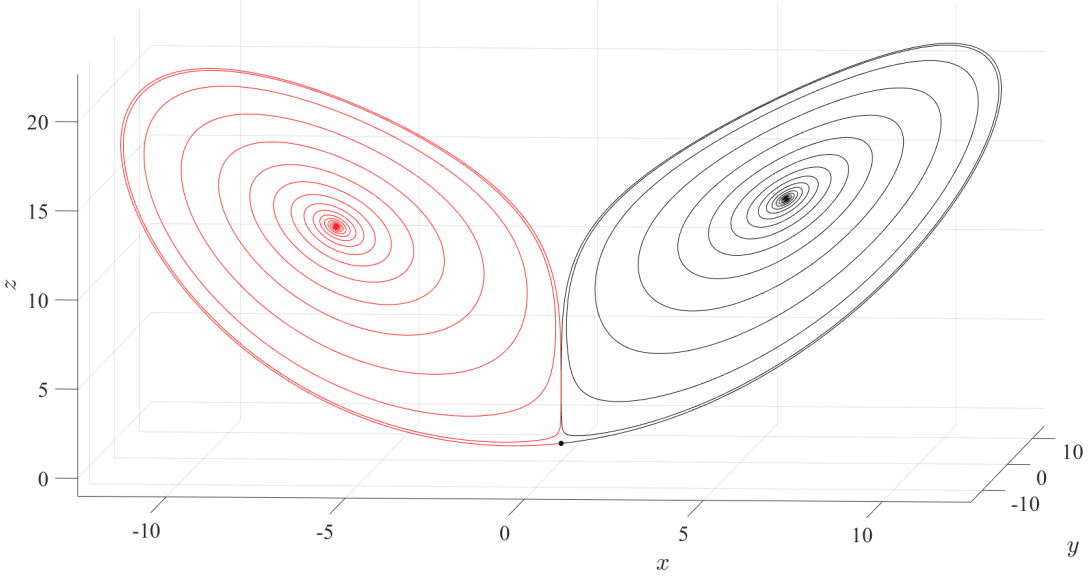


Figure 15: Black curve: initial conditions $(10^{-16}, 10^{-16}, 10^{-16})$, red curve: initial conditions $(10^{-16}, -10^{-16}, 10^{-16})$. Parameter values $(\sigma, \beta, \rho) = (10, \frac{8}{3}, 13.926)$.

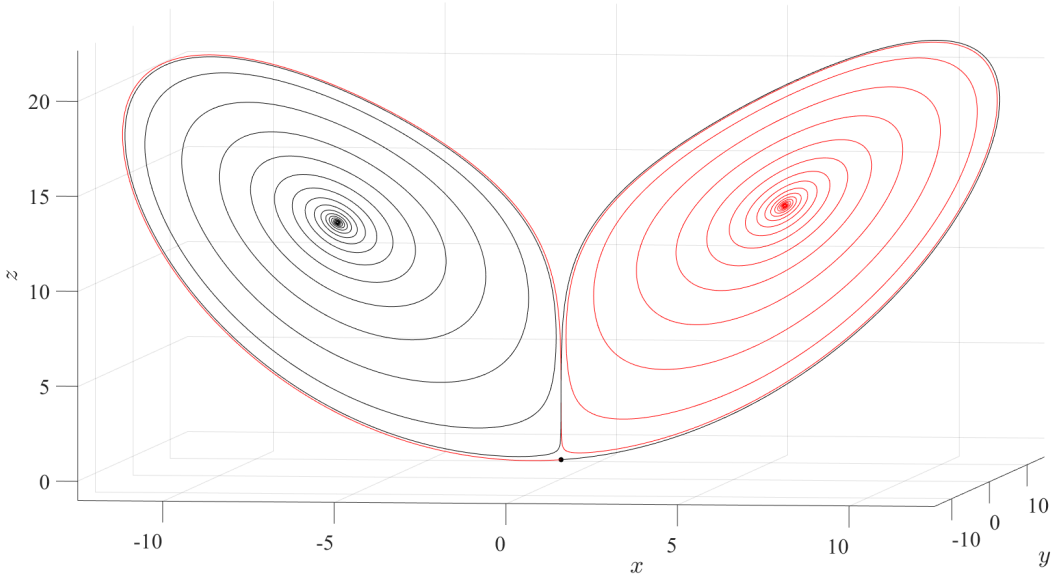


Figure 16: Black curve: Initial conditions $(10^{-16}, 10^{-16}, 10^{-16})$, red curve: Initial conditions $(10^{-16}, -10^{-16}, 10^{-16})$. Parameter values $(\sigma, \beta, \rho) = (10, \frac{8}{3}, 13.927)$.

Figure 15 and Figure 16 experimentally capture the behaviour illustrated schematically in Figure 13 and Figure 14. Therefore we can conclude that $\rho_b = 13.926\dots$ for the stated parameter values used. This drastic behaviour change can be partially explained by the touching of the two manifolds of the origin at $\rho = \rho_b$.

We conclude by the uniqueness of trajectories that the two manifolds must touch along the entire length of the unstable manifold, ruling out isolated point contact. Thus, any trajectory starting on the unstable manifold of the origin also lies in the stable manifold and will initially project away from the origin in the direction associated with the unstable eigenvalue before spiralling around either C^+ or C^- , then returning to the saddle point at the origin in the plane created by the eigenvectors associated with the stable eigenvalues. This behaviour occurs both as $t \rightarrow -\infty$ and $t \rightarrow \infty$. We call this loop associated with the fixed point at the origin a homoclinic orbit. Figure 17 shows a visual representation of the homoclinic orbits.

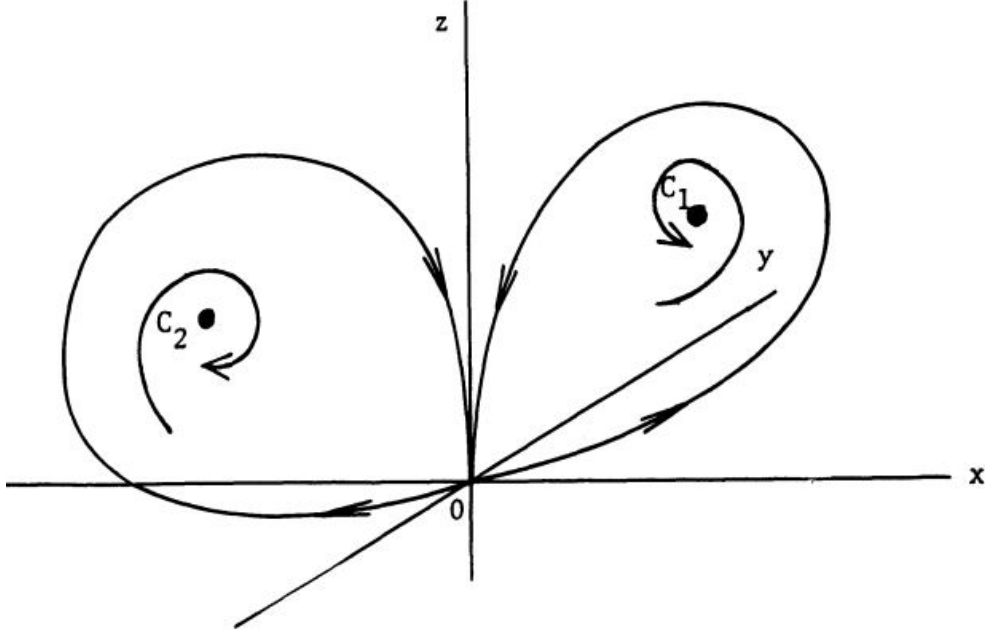


Figure 17: Homoclinic orbits at $\rho = \rho_b$. [14]

Summarising the challenging behaviour in this section:

- For $1 < \rho < 13.926\dots$ there are no limit cycles and trajectories settle down to either C^+ or C^- depending on their starting point relative to the stable manifold of the origin.
- For $\rho = 13.926\dots$ there is a homoclinic orbit associated with the saddle point at the origin due to the touching of the stable and unstable manifolds of the origin.
- For $\rho > 13.926\dots$ a pair of unstable limit cycles is created.
- The qualitative change in behaviour that occurs when increasing ρ through $\rho_b \approx 13.926$ indicates the existence of a homoclinic bifurcation at ρ_b .

2.3.6 Transient Chaos and Two Types of Attractor

We have already seen that in the case of $\sigma = 10$ and $\beta = \frac{8}{3}$, limit cycles are created as ρ increases past 13.926. Now we will further investigate the behaviour of trajectories for values of ρ between 13.926 and $\rho \approx 24.74 = \rho_H$, where C^+ and C^- become unstable.

Experimenting with different values of $\rho > 13.926$ shows that the limit cycle produces immediately smaller orbits around the equilibrium point it is attracted to if ρ is larger, however, the time spent oscillating around the fixed point before settling down increases with ρ . Figure 18 and Figure 19 demonstrate this behaviour.

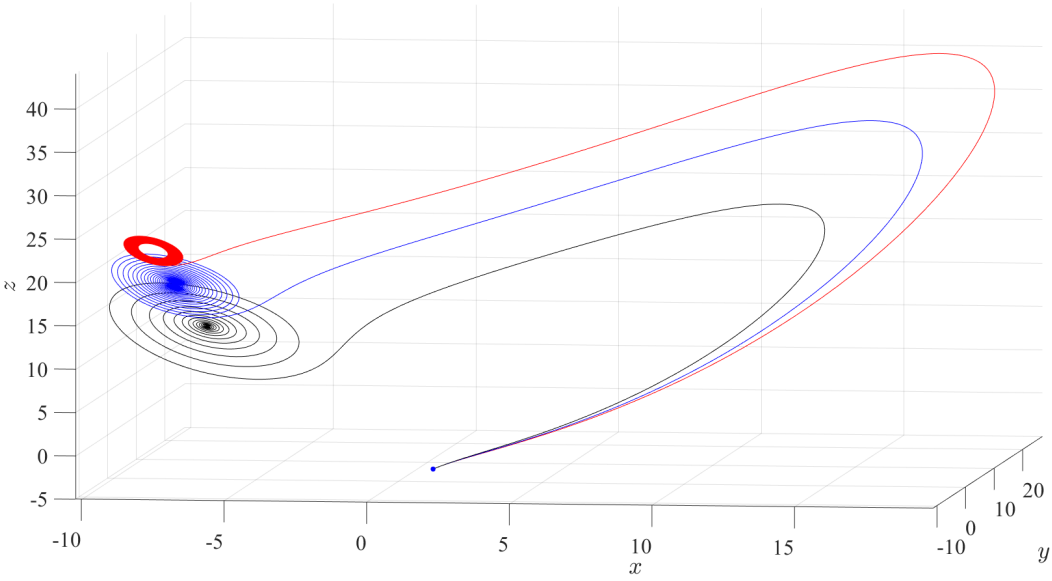


Figure 18: Initial conditions $(1, 2, -4)$. Parameter values $(\sigma, \beta, \rho) =$ black: $(10, \frac{8}{3}, 15)$; blue: $(10, \frac{8}{3}, 20)$; red: $(10, \frac{8}{3}, 24)$.

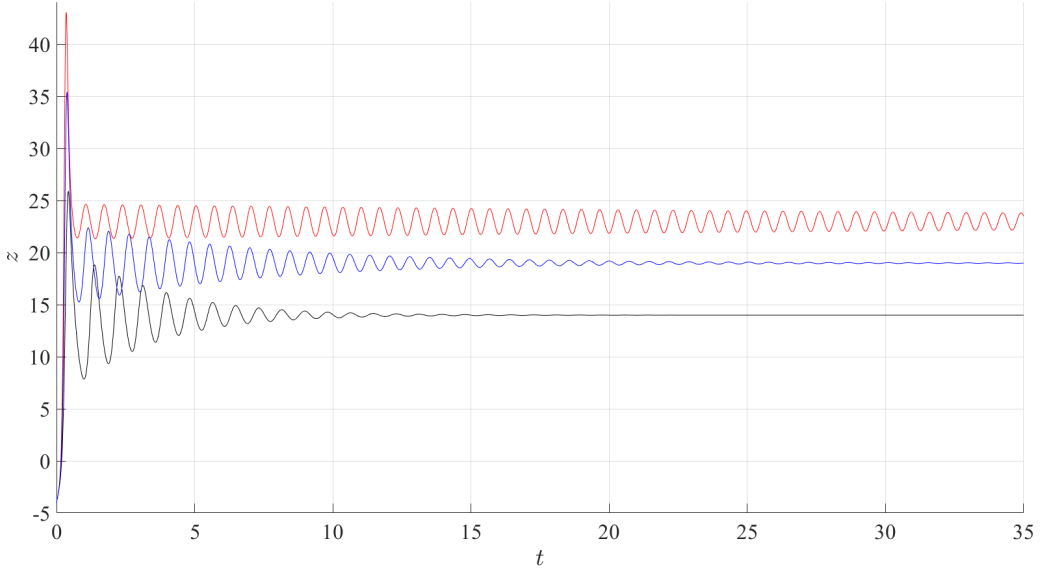


Figure 19: Time series of z against t . Initial conditions $(1, 2, -4)$. Parameter values $(\sigma, \beta, \rho) =$ black: $(10, \frac{8}{3}, 15)$; blue: $(10, \frac{8}{3}, 20)$; red: $(10, \frac{8}{3}, 24)$.

A possible physical representation of this behaviour could be that ρ being relatively large in the range $\rho_b < \rho < \rho_H$ suggests a climate with more changeable but less severe weather when compared to lower values of ρ in the same range. This is because the red trajectory (large ρ) in Figure 19 has sustained, low-amplitude oscillations, whereas the black (small ρ) trajectory has relatively high amplitude initial oscillations before diminishing fairly quickly. This interpretation is drawn from the fact that the Lorenz system is essentially a

simplified weather model.

For $13.926 < \rho < 24.06$, certain initial conditions also give rise to a behaviour categorised as transient chaos. The long-term behaviour of trajectories is not aperiodic, thus we cannot call it chaos in the traditional sense, however, the trajectories still display sensitive dependence on initial conditions for certain starting points. Figure 20 shows this behaviour for trajectories differing only by 10^{-5} in the y -direction. After some initial chaotic-looking oscillations, the trajectories eventually escape to the attracting basin of either C^+ or C^- depending sensitively on the initial condition; and settle down at one of the stable equilibrium points. Despite only a slight change in initial conditions, the trajectories shown converge to opposite equilibrium points, highlighting the term transient chaos.

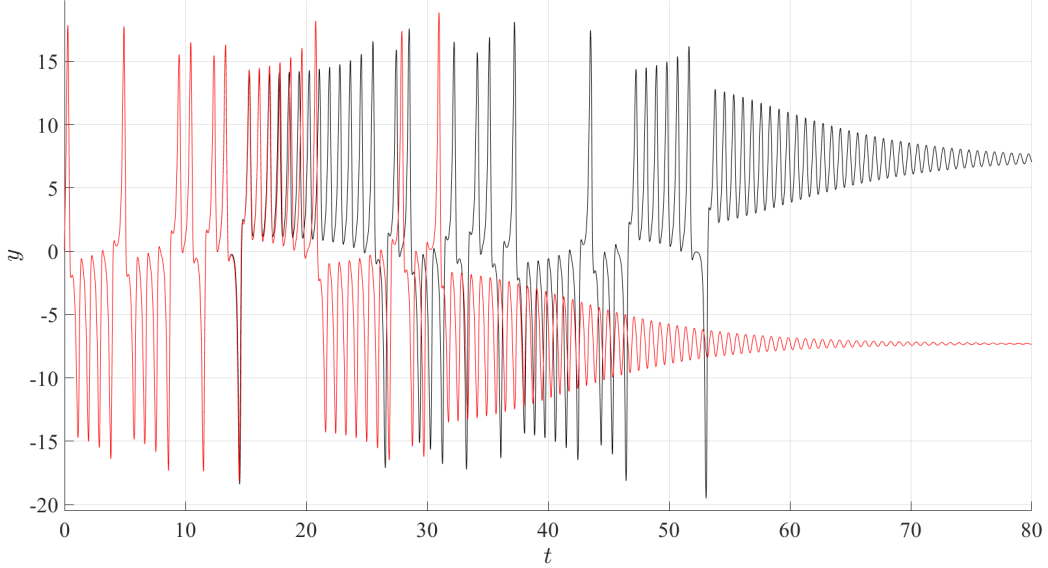


Figure 20: Time series of y against t showing transient chaos. Initial conditions: black = $(5, 0, 5)$; red = $(5, -10^{-5}, 5)$. Parameter values $(\sigma, \beta, \rho) = (10, \frac{8}{3}, 21)$

Transient chaos demonstrates that a deterministic system can exhibit unpredictability, even when its eventual outcomes are straightforward. In particular, strange attractors are not necessary to produce effectively random behaviour. This phenomenon mirrors experiences in everyday life; for instance, many gambling games serve as examples of transient chaos. Consider the act of flipping a coin: while the coin will inevitably settle into one of two stable positions, predicting the outcome proves challenging due to its sensitivity to initial conditions such as orientation and velocity.

Two types of attractors exist for $24.06 < \rho < 24.74$; fixed points and the strange attractor. Perhaps the easiest way to represent the system's dynamics for this set of values of ρ is by using a one-dimensional return map. In Figure 21, a “trajectory” on the map is a sequence of points obtained by repeated application of the map to some initial point - also known as cobwebbing.

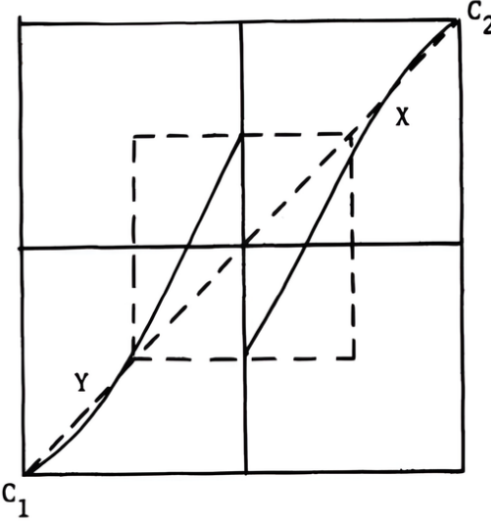


Figure 21: One-dimensional return map for the Lorenz flow. $24.06 < \rho < 24.74$. [14]

In Figure 21, C_1 and C_2 represent C^- and C^+ , respectively, and X, Y represent two boundaries which divide the phase space into different basins of attraction. Trajectories starting between X and C_2 tend towards C_2 , while trajectories starting between Y and C_1 tend towards C_1 . Trajectories starting between X and Y converge to the dotted box, which contains the strange attractor. Once within the box, trajectories remain there for an infinite time. The presence of these three attracting sets divides the phase space into three basins of attraction.

As we have now studied the most important behaviours as ρ varies in the Lorenz system, we can again create a simplified bifurcation diagram which adds more detail than the one shown in Figure 5. This is depicted in Figure 22.

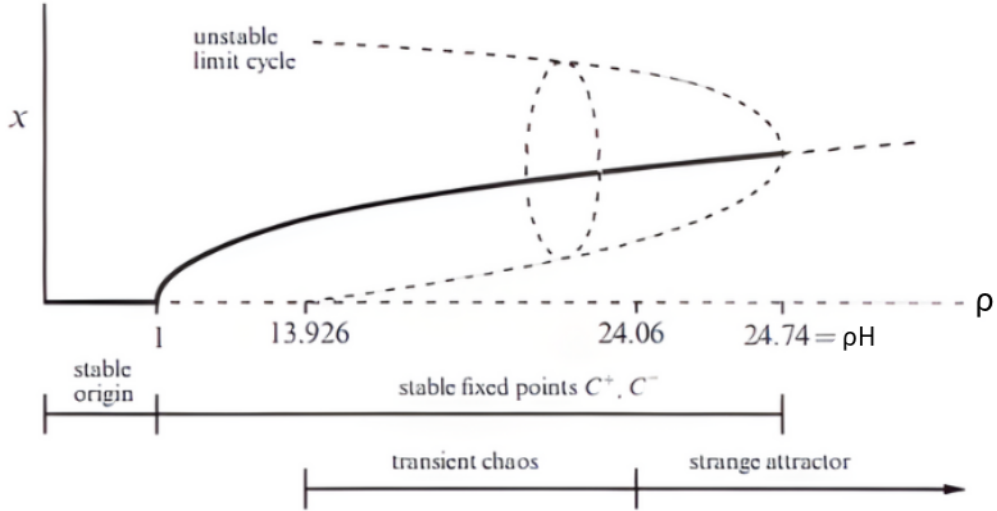


Figure 22: Simplified bifurcation diagram for ρ in the Lorenz system. $\sigma = 10, \beta = \frac{8}{3}$. [11]

2.3.7 Beyond the Hopf Bifurcation

As previously established, when ρ increases to 24.74 in the case of $\sigma = 10$ and $\beta = \frac{8}{3}$, there is a Hopf bifurcation. By this point, the Lorenz system already demonstrates chaos in the form of the strange attractor and

one might expect that this behaviour exists for all values of $\rho > \rho_H$. This is however not true in all cases. For most values of ρ between 24.74 and 313, the system exhibits chaos, though there are some small windows of periodic behaviour interspersed - the three largest of these being $99.524 < \rho < 100.795$, $145 < \rho < 166$ and $\rho > 214.4$ [11].

3 Applications of Chaos

3.1 Chaotic Masking

Chaos itself has many applications in various fields such as engineering, robotics, biology, stocks and more. However, due to its relatively recent emergence, the usefulness of chaos theory has been questioned with further exploration needed to harness its potential in the real world.

Kevin Cuomo was among the first to utilise chaos for a specific purpose when he used the chaotic behaviour produced by the Lorenz equations to transmit a private message in a demonstration involving the concepts of synchronised chaos and chaotic masking, building on a paper by Pecora and Carroll (1990) [15]. Before this paper, many doubted that two chaotic systems could synchronise due to their sensitive dependence on initial conditions.

In his experiment, Cuomo meticulously constructed a circuit comprising resistors, capacitors, operational amplifiers (op-amps) and analogue multiplier chips such that the voltages measured at three distinct points of the circuit gave values proportional to the Lorenz system's parameters ($x(t)$, $y(t)$, $z(t)$). The circuit acted as an analogue computer for the equations with each component responsible for different aspects of the system. The resistor values chosen set the constant parameters, the op-amps were configured as integrators and summing junctions to allow the solutions to be outputted as a voltage, while the analogue multiplier chips enabled the existence of the non-linear terms in the system. Figure 23 shows a schematic diagram of the circuit Cuomo used for the experiment.

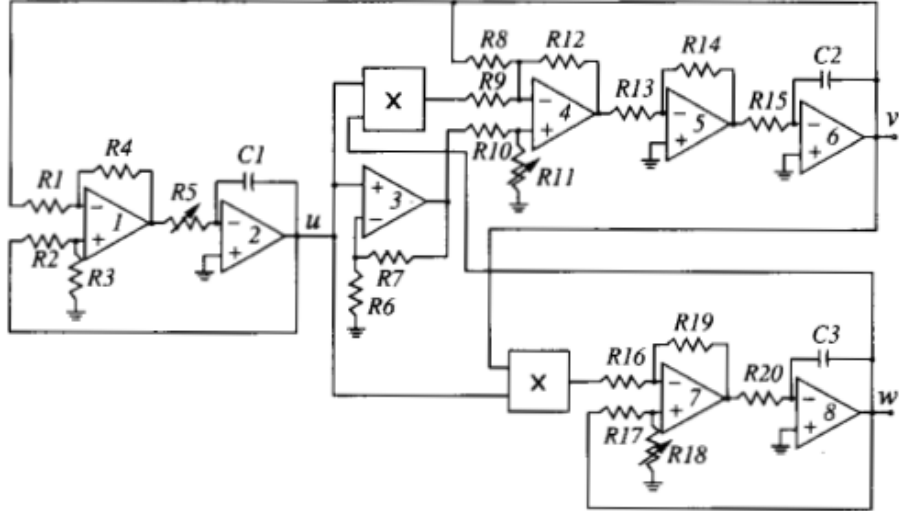


Figure 23: Lorenz-based chaotic circuit. [16]

Once set up, Cuomo was able to view the strange attractor by connecting the circuit to an oscilloscope, as depicted in Figure 24.

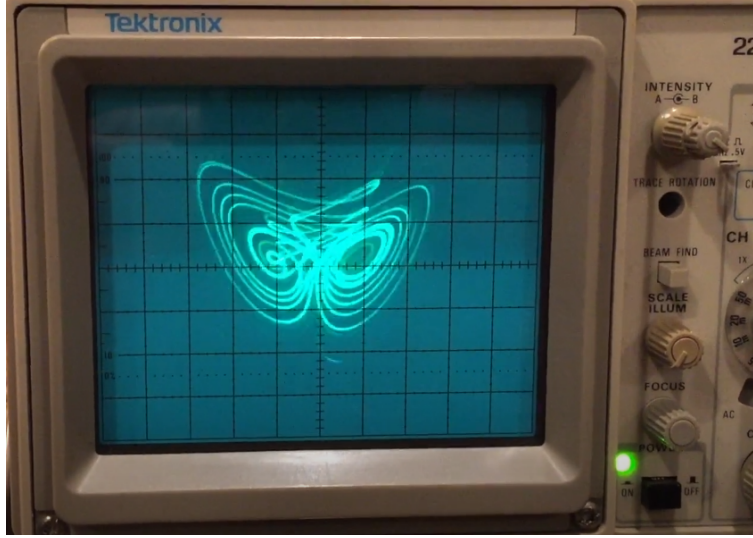


Figure 24: The Lorenz attractor viewed on an oscilloscope.

Furthermore, connecting the circuit to an amplifier generated a noise which sounded like radio static, as perhaps might have been expected in a chaotic circuit.

Cuomo then set up a second, near-identical circuit and used one as a transmitter and the other as the receiver. Then, by only using the x data from the transmitter circuit, the receiver circuit cleverly synchronised its behaviour with the solutions from the transmitter circuit despite having only one-third of the information from the first circuit being sent over. Let $\mathbf{d} = (x(t), y(t), z(t))$ be the three voltages measured in the transmitter (or driver) circuit and $\mathbf{r} = (x_r(t), y_r(t), z_r(t))$ be the corresponding voltages in the receiver circuit. We can check that synchronised chaos is occurring by plotting $x_r(t)$ and $y_r(t)$ against $x(t)$ and $y(t)$, respectively. These plots, depicted in Figure 25, show a straight line of slope 1, indicating a near-perfect synchronisation of the two chaotically running circuits.

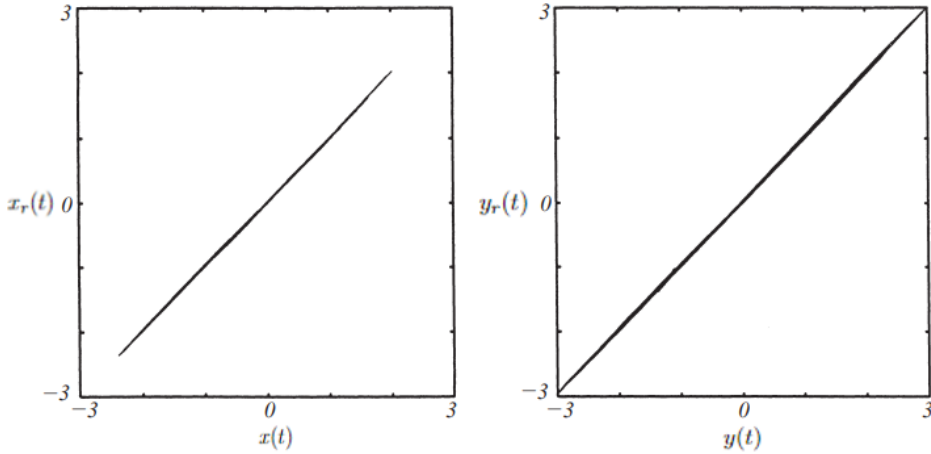


Figure 25: Circuit data showing synchronisation of circuits. $x_r(t)$ vs $x(t)$ (left); $y_r(t)$ vs $y(t)$ (right). [16]

The only difference between the circuits is that the drive signal $x(t)$ replaces the receiver signal $x_r(t)$ at a crucial place in the receiver circuit. Now, using Kirchoff's laws and other circuit rules, the governing equations for the transmitter are found to be:

$$\dot{x} = \sigma(y - x)$$

$$\dot{y} = \rho x - y - xz$$

$$\dot{z} = xy - \beta z$$

familiarly recognised as the Lorenz equations. The receiver circuit is governed by the same equations, however, we replace $x_r(t)$ with the $x(t)$ signal from the transmitter which drives the receiver circuit in the equations for \dot{y} and \dot{z} . Hence the equations for the receiver circuit are:

$$\dot{x}_r = \sigma(y_r - x_r)$$

$$\dot{y}_r = \rho x(t) - y_r - x(t)z_r$$

$$\dot{z}_r = x(t)y_r - \beta z_r$$

To show that these circuits synchronise, we consider the error vector of voltages between the two circuits $\mathbf{e} = \mathbf{d} - \mathbf{r} = (x - x_r, y - y_r, z - z_r) = (e_x, e_y, e_z)$ and show that $\mathbf{e}(t) \rightarrow \mathbf{0}$ as $t \rightarrow \infty$. The error dynamics can be written as follows:

$$\dot{e}_x = \sigma(e_y - e_x)$$

$$\dot{e}_y = -e_y - x(t)e_z$$

$$\dot{e}_z = x(t)e_y - \beta e_z$$

This is a non-autonomous linear system for $\mathbf{e}(t)$ with a possibly chaotic time-dependent coefficient $x(t)$ appearing in two terms. To get rid of these coefficients we can manipulate the equations in the following way:

$$\begin{aligned}\dot{e}_y e_y + \dot{e}_z e_z &= -e_y^2 - xe_y e_z + xe_y e_z - \beta e_z^2 \\ &= -e_y^2 - \beta e_z^2\end{aligned}$$

Now we no longer have the chaotic coefficient. Notice that the left-hand side equals

$$\frac{d}{dt} \left(\frac{1}{2} (e_y^2 + e_z^2) \right)$$

which helps us construct a Lyapunov function to show that $\mathbf{e} \rightarrow \mathbf{0}$. Consider,

$$V(t) = \frac{1}{2} \left(\frac{1}{\sigma} e_x^2 + e_y^2 + e_z^2 \right)$$

then V is positive definite ($\sigma > 0$) as it is the sum of squares. We must also show that \dot{V} is negative definite.

$$\begin{aligned}\dot{V} &= \frac{1}{\sigma} e_x \dot{e}_x + e_y \dot{e}_y + e_z \dot{e}_z \\ &= -(e_x^2 - e_x e_y) - e_y^2 - \beta e_z^2\end{aligned}$$

Completing the square for the bracketed terms yields

$$\begin{aligned}\dot{V} &= -\left(e_x - \frac{1}{2}e_y\right)^2 + \left(\frac{1}{2}e_y\right)^2 - e_y^2 - \beta e_z^2 \\ &= -\left(e_x - \frac{1}{2}e_y\right)^2 - \frac{3}{4}e_y^2 - \beta e_z^2\end{aligned}$$

Thus, $\dot{V} \leq 0$ with equality only if $\mathbf{e} = \mathbf{0}$. We therefore conclude that V is a Lyapunov function and the Lyapunov stability theorem implies that $\mathbf{e} = \mathbf{0}$ is globally asymptotically stable, that is $\mathbf{e} \rightarrow \mathbf{0}$.

In Cuomo's actual experiment, he used the circuits to mask a message. In particular, he played a chaotically masked version of the song "Emotions" by Mariah Carey which sounded like a hiss due to the chaotic signal produced by the driver circuit being roughly 20 decibels louder than the original song. However, when the signal was sent to the receiver circuit, its output synchronised almost perfectly with the original chaos and, after electronic subtraction, the original song could be heard, albeit slightly muffled.

3.2 Controlling Chaos

3.2.1 The OGY Method

Chaos control refers to the manipulation and stabilisation of chaotic systems, a concept first introduced in 1990 by a paper written by Ott, Grebogi and Yorke from the University of Maryland [17]. In the paper, instead of viewing chaos as infinite aperiodic behaviour, the authors looked at it as an infinite number of unstable periodic orbits and attempted to exploit this by using a specific method (the OGY method) to control a chaotic attractor. The method consists of applying small perturbations to the system at precise times once per 'cycle' to guide the system away from chaotic behaviour and stabilise a chosen unstable periodic orbit with desirable properties for the intended application.

The method can be applied to n -dimensional continuous-time systems but for the sake of simplicity, we can treat the problem as though it were in discrete time. That is, we study the behaviour of trajectories of a chaotic orbit piercing a chosen Poincaré section. There will be an infinite number of piercings, where one of these will represent the desired unstable periodic orbit. This is an unstable fixed point of the Poincaré return map. Suppose this return map can be represented by

$$\mathbf{x}_{i+1} = f(\mathbf{x}_i, p)$$

where $\mathbf{x}_i \in \mathbb{R}^n$ is the n -dimensional state of the system at iteration i and p is a parameter of the system. Now let the unstable periodic orbit be represented by \mathbf{x}^* . Then in the neighbourhood of \mathbf{x}^* , you have both the points \mathbf{x}_i and \mathbf{x}_{i+1} where you can relate the distances between \mathbf{x}_{i+1} and \mathbf{x}_i to \mathbf{x}^* as the function

$$(\mathbf{x}_{i+1} - \mathbf{x}^*) = A(\mathbf{x}_i - \mathbf{x}^*) + B(p - \bar{p})$$

The function considers both dependence on the state and the parameter where A and B are the matrices obtained when $f(\mathbf{x}_i, p)$ is differentiated with respect to \mathbf{x}_i and p , respectively. Thus, A is the Jacobian matrix and \bar{p} is the parameter value for which \mathbf{x}^* was obtained. Now assume that it is possible to change the parameter by a small amount in each iteration so that the perturbation in the parameter should be dependent on some constant controllability matrix, K , multiplied by the deviation in the state, as shown below. Note that K is obtained using techniques from control theory which will not be discussed here.

$$(p_i - \bar{p}) = -K^T(\mathbf{x}_i - \mathbf{x}^*)$$

A transpose is applied to the matrix for dimensional consistency. Now, substituting this equation into the previous one and replacing $(\mathbf{x}_i - \mathbf{x}^*)$ with $\delta\mathbf{x}_i$ yields

$$\delta\mathbf{x}_{i+1} = (A - BK^T)\delta\mathbf{x}_i$$

Hence, an initial deviation, $\delta\mathbf{x}_i$, from the unstable periodic orbit yields a final deviation of $\delta\mathbf{x}_{i+1}$ after one iteration, supposing you apply a parameter perturbation of $(p_i - \bar{p})$. Now, we observe that the only condition

for stability is the matrix $(A - BK^T)$ must have eigenvalues inside the unit circle ($|\lambda_j| < 1$, for all j). This ensures that in successive iterations, the deviation will converge to $\mathbf{0}$.

Another thing to mention is that we only apply the parameter perturbation when $\delta\mathbf{x}_i$ is sufficiently small, that is, we wait until the state falls in a close neighbourhood of \mathbf{x}^* to apply the perturbation so that the system ‘locks’ onto the unstable periodic orbit. This is for two reasons:

1. We only want to apply a small perturbation to the parameter due to the volatile nature of chaotic systems.
2. The linearised dynamics of the system will only be valid in the neighbourhood of the equilibrium point.

The OGY algorithm also works for orbits with periods greater than one, though the process is slightly more complicated and involves stabilising eigenvectors in unstable directions.

3.2.2 OGY Method and Delay Coordinates

Suppose you wanted to study an n -dimensional continuous-time chaotic system. It is often not possible to measure all n state components, but only one or two. We have to modify the OGY method for this circumstance using delay coordinates. The basic idea of delay-coordinate embedding is to plot the time series data of one state variable (say x) against delayed versions of itself. The chaotic attractor can then be reconstructed by defining n new states $x(t), x(t-\tau), x(t-2\tau), \dots, x(t-(n-1)\tau)$, where τ is a suitably chosen delay time. It is important to note that *Takens’ Theorem* [18] places restrictions on τ and the number of dimensions considered in the ‘reconstruction space’ exist, but we will not go into detail here.

Figure 26 shows an example of the reconstructed Lorenz attractor in Python using delay-coordinate embedding with only the x -data from the system.

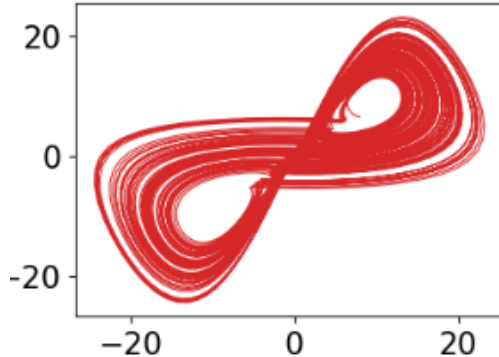


Figure 26: Lorenz attractor reconstruction using delay coordinates $(x(t), x(t-\tau))$, $\tau = 10$. [19]

To apply delay coordinates to the OGY algorithm, assume we are dealing with discrete time intervals obtained from a Poincaré map of a continuous-time system. The delay coordinate defined as

$$X(t_i) = [x(t_i), x(t_i - \tau), \dots, x(t_i - (n-1)\tau)]$$

at time t_i includes not only the current state $x(t_i)$ but also its previous states $x(t_i - \tau), x(t_i - 2\tau), \dots$ which help to capture the system’s dynamics over time.

Now denote the time between successive intersections of the solution trajectory with the Poincaré map as t_F . Should this interval be shorter than the period required for the system to ‘fade its memory’ of past states, expressed as $(n-1)\tau > t_F$, then the delay coordinate at time t_i retains information about the preceding intersection at $t_i - t_F$. Consequently, any perturbations introduced to the system at $t_i - t_F$ persist and influence its behaviour at t_i .

Hence, all parameter values $\{p_i, \dots, p_{i-r}\}$ have an influence on the variable $X(t_i)$ where r signifies the smallest integer satisfying $(n-1)\tau < rt_F$. The system can therefore be described as:

$$X_{i+1} = F(X_i, p_i, p_{i-1}, \dots, p_{i-r})$$

where $X(t_i) = X_i$. Now the linearisation is slightly different. We have:

$$X_{i+1} - X_{i+1}^* = A_i(X_i - X_i^*) + B_i^1(p_i - \bar{p}) + B_i^2(p_{i-1} - \bar{p}) + \dots + B_i^{r+1}(p_{i-r} - \bar{p})$$

where $B_i^j = D_{p_{i-(j-1)}} F(X, p_i, p_{i-1}, \dots, p_{i-r})$ and D_{p_i} denotes the derivative with respect to p_i .

In the linearisation above, p_i is the only unknown on the right-hand side which we can solve for by introducing new variables:

$$Y_i = \begin{pmatrix} X_i \\ p_{i-1} \\ p_{i-2} \\ \vdots \\ p_{i-r} \end{pmatrix} \quad \text{and} \quad Y_i^* = \begin{pmatrix} X_i^* \\ \bar{p} \\ \bar{p} \\ \vdots \\ \bar{p} \end{pmatrix}$$

$$\tilde{A}_i = \begin{pmatrix} A_i & B_i^2 & B_i^2 & \cdots & B_i^r & B_i^{r+1} \\ \mathbf{0} & 0 & 0 & \cdots & 0 & 0 \\ \mathbf{0} & 1 & 0 & \cdots & 0 & 0 \\ \mathbf{0} & 0 & 1 & \cdots & 0 & 0 \\ \vdots & \vdots & \vdots & \ddots & \vdots & \vdots \\ \mathbf{0} & 0 & 0 & \cdots & 1 & 0 \end{pmatrix} \quad \text{and} \quad \tilde{B}_i = \begin{pmatrix} B_i^1 \\ 1 \\ 0 \\ \vdots \\ 0 \end{pmatrix}$$

With these new variables and matrices [20], the linearisation can be written to resemble the form from the previous section:

$$(Y_{i+1} - Y_{i+1}^*) = \tilde{A}_i(Y_i - Y_i^*) + \tilde{B}_i(p_i - \bar{p})$$

The new matrices \tilde{A}_i and \tilde{B}_i can then be used in the OGY algorithm described in the previous section.

3.2.3 Estimation Techniques in the OGY Algorithm

We have so far looked at the OGY method where A , B and the fixed points of the Poincaré map are known. However, these often need to be estimated. This section will give a very brief overview of how one might tackle these issues. Details will be kept to a minimum and can be explored in another project.

Implementing the OGY method to control a chaotic system can be broken down into several fundamental steps:

1. Define a suitable delay coordinate and construct a Poincaré map to create $X(t_i) = [x(t_i), x(t_i - \tau), \dots, x(t_i - (n-1)\tau)]$.
2. Find fixed points $X(t_{i+1}) = X(t_i)$ and period T points $X(t_{i+T}) = X(t_i)$ of the Poincaré map using the recurrence method (described below).
3. Linearise the Poincaré map in the neighbourhood of these points and apply a least squares method to find A .
4. Apply a parameter perturbation and linearise again around the fixed points to find B .

The recurrence method can estimate fixed points of the Poincaré map of a chaotic system. It relies on finding points that return to a similar state after a specific number of iterations. Hence, lots of sample data points are required which are obtained by repeatedly iterating the system's equations.

Take $p = \bar{p}$, then define a vicinity threshold, ϵ . Points that fall within ϵ distance of a previously generated point, x_i , after m iterations of the Poincaré map are considered (m, ϵ) recurrence points. That is, for each point, x_i , follow its images x_{i+1}, x_{i+2}, \dots until the smallest k is found such that $|x_k - x_i| < \epsilon$ ($m = k - i$). This indicates a possible period- m orbit. More data points and a smaller vicinity threshold lead to a higher accuracy of the recurrence method.

Points representing the same Poincaré point based on their recurrence profile are then grouped and averaged. The resulting sequence of points provides an appropriate estimation of the fixed points of the Poincaré map.

Using the data obtained from the recurrence method, a least squares method is used to estimate the matrix A . Fundamentally, the least squares method involves finding a best-fit linear curve for a function $y = ax + c$ for which the sum of squares of the errors of each point $e_j = y_j - (ax_j + c)$ is minimised over all points (x_j, y_j) . The technique extends to n dimensions and can be applied to estimate A . Estimating B involves repeating the recurrence procedure and least squares method for a perturbed parameter value.

3.3 Applications of Chaos Control

3.3.1 Cardiac Chaos Control and Targeting

The OGY method is not the only method of chaos control. We have already seen synchronised chaos - a form of controlling chaos - through Cuomo's experiment. There is also the *Pyragas method* which (like the OGY method) aims to stabilise a periodic orbit. However, unlike the OGY method, it involves providing a continuous controlling signal to a chaotic system, whose intensity is almost zero as the system evolves close to the desired periodic orbit and becomes larger when moving away from the periodic orbit.

Applications of chaos control are numerous and, with the rapid rise of artificial intelligence, techniques in reinforcement learning can be used to solve these controllability problems efficiently and with great accuracy. For example, the double pendulum is a notoriously chaotic system involving a pendulum with a second pendulum attached to its end. This video from the Technical University of Vienna <https://www.youtube.com/watch?v=B6vr1x6KDaY> [21] shows a neural network trained to stabilise the double pendulum in the upright position (unstable equilibrium), demonstrating chaos control in action.

A critical application of chaos control lies in addressing cardiac issues in humans. As an individual approaches cardiac failure, the dynamics of the heartbeat shift from stable periodic orbits to unstable periodic orbits and chaos. The natural question is then can this chaos be controlled and the heartbeat restabilised?

For certain heart conditions such as ventricular fibrillation, one method presently used to tackle this issue is to insert a device underneath the clavicle called an implantable cardioverter defibrillator (ICD). Thin wires connect the ICD to the heart, where it continuously monitors heart rate and rhythm using electrodes [22]. When the ICD detects an erratic heartbeat, it delivers an electric shock to restore normal rhythm. The intensity of these shocks can vary depending on the nature of the arrhythmia, with large, painful shocks being required more frequently than desired. These powerful shocks may cause the death of some cardiac tissues. Therefore, the idea of using chaos control in cardiac care is to deliver smaller, precisely timed electrical impulses to prevent these painful instances, whilst still effectively managing irregular rhythms.

Successful experiments involving methods of chaos control have been performed on an isolated portion of a rabbit heart [17], resulting in a stable heartbeat. Consequently, researchers are optimistic that the same technique can be applied to humans. However, there is a challenge to overcome. If the state of the heartbeat is far away from the desired periodic orbit, so far we have waited until the system naturally approaches the

periodic orbit before applying a perturbation to control the chaos. This is impractical in humans experiencing arrhythmia as waiting could result in fatal outcomes. Hence, a question arises: can we bring a state quickly to a desirable state?

As it turns out, this capability is possible, and unique to chaotic systems. This is because in other systems, a significant shift in the state typically requires a large parameter perturbation. However, the sensitive nature of chaotic systems allows a small change in a parameter to drastically influence the state of the system. This concept of transitioning quickly between widely spread states is known as chaotic targeting and there is no equivalent process in non-chaotic systems.

An effective way to illustrate targeting simply is through the logistic map. This is a straightforward map given by the equation $x_{n+1} = f_r(x_n) = rx_n(1 - x_n)$ which is chaotic for values of $r > 3.57$. Suppose for an initial condition $x_0 = 0.4$, we wish to target the point $x = 0.8$ in as few iterations as possible. Assume that the default parameter value is $r_0 = 3.9$ and that we can perturb the parameter slightly at each iteration with an allowed parameter range of $3.8 < r < 4.0$. Figure 27 shows an example cobweb diagram for this situation with the curves drawn with parameter values of 3.8 and 4.0.

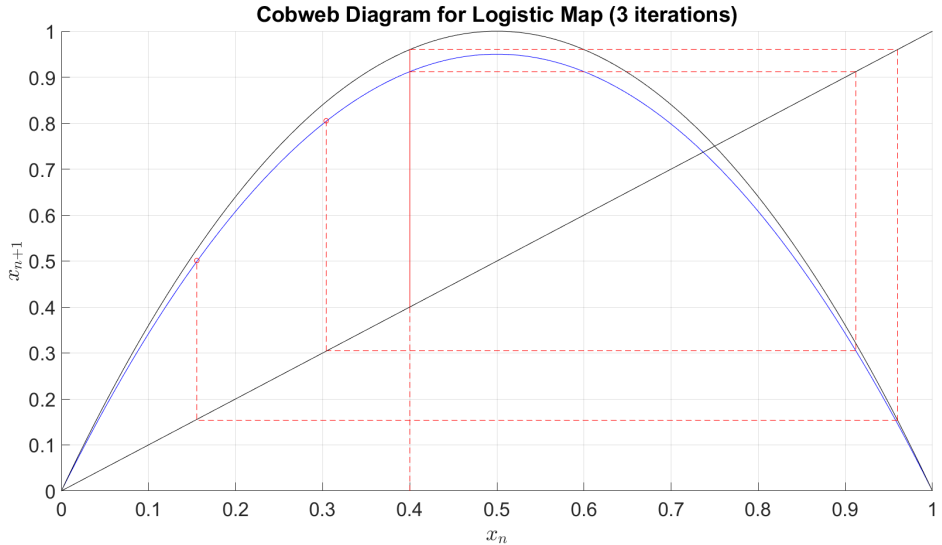


Figure 27: Cobweb diagram for the logistic map, $x_{n+1} = f_r(x_n) = rx_n(1 - x_n)$. Values of r : blue curve = 3.8; black curve = 4.0.

From the diagram, we observe that $x_1 \in f_{[3.8,4.0]}(0.4) = [0.91, 0.96]$. Then, reverting the parameter to $r = 3.9$ for the sake of simplicity, we have,

$$x_2 \in f_{3.9}([0.91, 0.96]) = [0.1498, 0.3130]$$

$$x_3 \in f_{3.9}([0.1498, 0.3130]) = [0.4966, 0.8386]$$

Notice now that the target value of 0.8 lies in the range of x_3 . Now, since f_r is continuous with respect to r , the intermediate value theorem implies the existence of a parameter r such that

$$f_{3.9}(f_{3.9}(f_r(0.4))) = 0.8$$

Further work reveals that $r = 3.8319$. Hence we have found the correct parameter perturbation needed to go from state $x_0 = 0.4$ to $x_3 = 0.8$ in only three iterations. This example highlights how a small, deliberate perturbation can rapidly guide a chaotic system to the desired location. Hence, sensitive dependence on

initial conditions can be useful in designing a responsive control system.

In theory, this method can be adapted and used to modify ICDs so that small, judiciously chosen parameter perturbations can quickly restabilise a human heart experiencing ventricular fibrillation. This would reduce the frequency of painful shocks received and avoid damage to cardiac tissues.

3.3.2 Chaotic Control in Space Travel

A real-life example of successful chaotic targeting was with the International Cometary Explorer (ICE) spacecraft [23]. Originally launched as The International Sun-Earth Explorer 3 (ISEE-3) in 1978, it aimed to investigate the interactions between solar wind (a stream of charged particles released from the sun) and Earth's magnetosphere.

It was first parked in a halo orbit about the Lagrange point L1 - a dynamically unstable fixed point in the Earth-moon system - then, in 1982, an opportunity arose to explore the comets Halley and Giacobini-Zinner, which were both entering the solar system. Despite having limited propellant, by using chaotic targeting, a viable orbit solution was eventually suggested.

On June 10, 1982, the spacecraft began a series of deliberate manoeuvres from its parked orbit around L1, which placed it on a transfer orbit involving passages around the Earth and the moon. In total, fifteen propulsive movements (and five lunar flybys) were made to get the spacecraft successfully to the two comets. ICE was the first spacecraft to investigate more than one comet.

This event underlined the importance of chaotic targeting and control as the success of this mission was only possible due to the chaotic nature of the restricted three-body problem - the spacecraft's motion in the presence of the earth and the moon - as well as the instability of L1.

Overall, we have seen that controlling chaos is an invaluable tool, with extremely promising applications in cardiology. We have also considered the influential role machine learning could play in the future of chaos control research as well as looking at a challenging scenario involving the restricted three-body which was solved via chaos control.

4 Conclusion

In conclusion, this project has investigated the Lorenz equations and some applications of chaos theory. Initially, we discussed the history of chaos theory by introducing the three-body problem before turning our attention to the Lorenz system; looking at the physical interpretation of parameters and its use as a simplified weather model for the Earth.

Through analysing the Lorenz equations, we highlighted the significance of sensitive dependence on initial conditions in a chaotic system - showing this through analytical and numerical investigations of parameters, especially ρ . We analysed the stability of steady states for different values of ρ , enabling us to create bifurcation diagrams to illustrate qualitative behaviour changes in the system.

After this analysis, we looked at Cuomo's electrical circuits (which replicated Lorenz equations) and their ability to synchronise chaos to send a private communication, before looking at other methods of chaos control (largely the OGY method). We also discussed the uses of chaos control in the human heart and space travel.

Ultimately, chaos theory is a relatively new field of mathematics which has seen rapid development, with new applications still being discovered. The advent of artificial intelligence and better computational powers promises to accelerate further progress. For instance, AI can extract underlying dynamics from historical

data, enabling the prediction of future states of chaotic systems. This has applications in weather forecasting, financial markets and other domains.

References

- [1] Cambridge.org. (2019). CHAOS — meaning in the Cambridge English Dictionary. [online] Available at: <https://dictionary.cambridge.org/dictionary/english/chaos>.
- [2] Hunt, B. and Yorke, J. (n.d.). Maxwell on Chaos. [online] Available at: https://yorke.umd.edu/Yorke_papers_most_cited_and_post2000/1993_04_Hunt_%20Nonlin-Science-Today%20_Maxwell%20on%20Chaos.PDF.
- [3] Wikipedia. (2021). Three-body problem. [online] Available at: https://en.wikipedia.org/wiki/Three-body_problem.
- [4] Barrow-Green, J. and Es, A. (1993). Poincare and the Three-Body Problem. [online] Available at: <https://oro.open.ac.uk/57403/1/335423.pdf> [Accessed 5 May 2024].
- [5] APS News (2003). This Month in Physics History. [online] Available at: <https://www.aps.org/publications/apsnews/200301/history.cfm#:~:text=With%20the%20advent%20of%20computers> [Accessed 5 May 2024].
- [6] Lorenz, E.N. (1963). Deterministic Nonperiodic Flow. Journal of the Atmospheric Sciences. [online] Available at https://journals.ametsoc.org/view/journals/atsc/20/2/1520-0469_1963_020_0130_dnf_2_0_co_2.xml.
- [7] Wikipedia. (2021). Lyapunov stability. [online] Available at: https://en.wikipedia.org/wiki/Lyapunov_stability.
- [8] Encyclopedia Britannica. (n.d.). Fundamental theorem of algebra. [online] Available at: <https://www.britannica.com/science/fundamental-theorem-of-algebra>.
- [9] Lopez, A.M. Different dynamical aspects of Lorenz system. [online] Available at: <https://diposit.ub.edu/dspace/bitstream/2445/127423/2/memoria.pdf> [Accessed 5 May 2024].
- [10] Izhikevich, E.M. (2007). Equilibrium. Scholarpedia. [online] Available at: <http://www.scholarpedia.org/article/Equilibrium>.
- [11] Strogatz, S (2018). NONLINEAR DYNAMICS AND CHAOS. Available at: https://www.biodyn.ro/course/literatura/Nonlinear_Dynamics_and_Chaos_2018_Steven_H._Strogatz.pdf.
- [12] Scientificlib. Attractor. [online] Available at: <https://www.scientificlib.com/en/Mathematics/DynamicalSystem/Attractor.html>.
- [13] Viswanath, D. (2004). The fractal property of the Lorenz attractor. Physica D: Nonlinear Phenomena. [online] Available at: <https://doi.org/10.1016/j.physd.2003.10.006>.
- [14] Sparrow, C. (1982). The Lorenz Equations: Bifurcations, Chaos, and Strange Attractors. Available at: <https://link.springer.com/book/10.1007/978-1-4612-5767-7>.

- [15] Pecora, L.M. and Carroll, T.L., 1990. Synchronization in chaotic systems. *Physical review letters*, 64(8), p.821. Available at: <https://doi.org/10.1103/PhysRevLett.64.821>.
- [16] Cuomo, K. (1993). Synchronization of Lorenz-B ased Chaotic Circuits with Applications to Communication. Available at: http://engineering.nyu.edu/mechatronics/Control_Lab/bck/VKapila/Chaotic%20Ref/Porfiri's/Biblio/cuomo93.pdf.
- [17] Ott, E. et al, (1990). Controlling Chaos, *Phys. Rev. Lett.* 64, 1196. [online] Available at: https://web.archive.org/web/20190227123431id_/http://pdfs.semanticscholar.org/8f55/8397236fc7a5059d7bb6a1cc14ec051c9afb.pdf.
- [18] Wikipedia Contributors (2024). Takens' theorem. [online] Wikipedia. Available at: https://en.wikipedia.org/wiki/Takens%27s_theorem [Accessed 5 May 2024].
- [19] Nauman, F. (2020). Julia Delay Embeddings: Lorenz [Notebook]. GitHub. Available at: https://github.com/fnauman/timeseries/blob/master/delayembedding/julia_delayembeddings_lorenz.ipynb.
- [20] Witvoet, G. (2005). Control of Chaotic Dynamical Systems using OGY. [online] Available at: <https://is.muni.cz/el/1431/jaro2016/M6201/um/OGY.pdf>.
- [21] Glueck, T. (2011). Double Pendulum on a Cart. [online] Available at: <https://www.youtube.com/watch?v=B6vr1x6KDaY>.
- [22] American Heart Association (2016). Implantable Cardioverter Defibrillator (ICD). [online] Available at: <https://www.heart.org/en/health-topics/arrhythmia/prevention--treatment-of-arrhythmia/implantable-cardioverter-defibrillator-icd>.
- [23] Rosenvinge, T. Brandt, J.C. and Farquhar, R.W. (1986). The International Cometary Explorer Mission to Comet Giacobini-Zinner. *Science*, 232(4748), pp.353–356. [online] Available at: <https://doi.org/10.1126/science.232.4748.353>.